Chapter 13

Optimization of CO_2 Sequestration in Saline Aquifers

Ramesh K. Agarwal and Zheming Zhang

Additional information is available at the end of the chapter

http://dx.doi.org/10.5772/57066

1. Introduction

For optimization of geological carbon sequestration (GCS) in saline aquifers, a genetic algorithm (GA) based optimizer has been developed and combined with the DOE multi-phase flow and heat transfer numerical simulation code TOUGH2 [1],[2]. Designated GA-TOUGH2, this combined solver/optimizer has been validated by performing optimization studies on a number of model problems and comparing the results with brute-force optimization, which requires a large number of simulations. Using GA-TOUGH2, an innovative reservoir engineering technique known as water-alternating-gas (WAG) injection has been investigated in the context of GCS, Additionally, GA-TOUGH2 has been applied to determine the optimal WAG operation for enhanced CO_2 sequestration capacity. GA-TOUGH2 is also used to perform optimization designs of time-dependent injection rate for optimal injection pressure management, and optimization designs of injection-well distribution for minimum well interference. The results obtained from these optimization designs suggest that over 50% reduction of in situ CO_2 footprint, greatly enhanced CO_2 dissolution, and significantly improved well injectivity can be achieved by employing GA-TOUGH2. The technique has also been employed to determine the optimal well placement in a multi-well injection operation. GA-TOUGH2 appears to hold great promise for studying a host of other optimization problems related to GCS.

2. Genetic algorithms

Genetic algorithms (GA) belong to a class of optimization techniques that are inspired by biological evolution [3],[4]. The algorithm begins with a set (identified as "generations") of vectors (identified as "individuals"). The individuals from one generation are used to create a new generation of individuals, which is supposed to be better than the previous generation.

Individuals used to form the next generation (identified as "offspring") are selected according to their function value in satisfying a certain criteria (identified as the "fitness function"). This process is repeated, creating the best individuals for each successive generation according to certain pre-defined criteria. Finally a generation of individuals is obtained where all the individuals in that generation produce the optimal values of the fitness function within a small tolerance. The algorithm is then considered to have achieved convergence. Detailed explanations of the GA can be found in Goldberg's book [4] and in our previous work [5].

3. GA-TOUGH2 integrated computer program

To realize the capability of numerical simulation and optimization for saline aquifer geological carbon sequestration (SAGCS), the GA optimizer is implemented in the TOUGH2 solver to obtain an integrated simulation-optimization computer program. Additional modules for pre- and post-simulation processes are introduced to enable the data sharing between GA and TOUGH2. A schematic of the program architecture and data flow is presented in Figure 1. Readers are encouraged to refer to our previous work for more details on the integrated code designated GA-TOUGH2 [6].

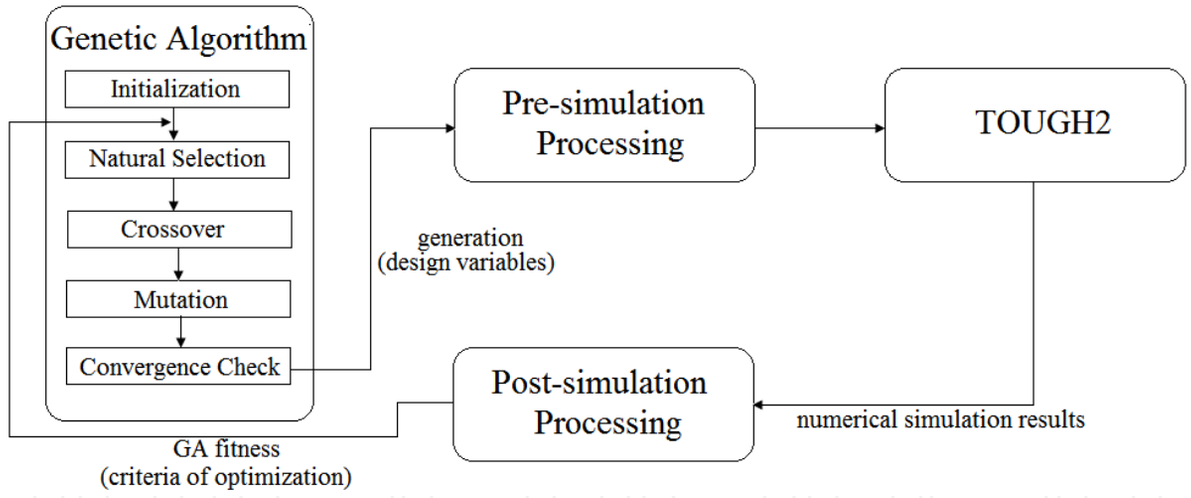

Figure 1. Graph of integrated GA-TOUGH2 code

4. Optimization of geological carbon sequestration in saline aquifers

The development of GA-TOUGH2 code and the successful simulation studies of GCS in large-scale saline formations have provided an understanding and the simulation tools for the study of optimization of some promising reservoir engineering techniques for more efficient and secure SAGCS practices. These optimization studies include (but are not limited to) the optimization of the constant-gas-injection rate for maximum CO_2 dissolution, the optimal

design of water-alternating-gas (WAG) injection schemes (patterns) for maximum storage efficiency, the design of optimum injection scenarios for optimal pressure management, and the optimal placement of wells in a multi-well injection system. Some of these optimization studies are described below.

4.1. Optimization of reduction in CO_2 plume migration for the water-alternating-gas (WAG) injection scheme

A reservoir engineering technique known as water-alternating-gas (WAG) scheme is considered for SAGCS for improving the sequestration efficiency, although additional injection of water with CO_2 will inevitably increase the cost. GA-TOUGH2 is employed to determine the optimal WAG operation for maximum CO_2 sequestration efficiency while minimizing water usage.

The idea of WAG operation was originally introduced in the oil industry to improve the sweeping efficiency during gas flooding of the oil reservoir. A significant amount of remaining oil could be recovered by regularly injecting intermittent slugs of water and gas (usually CO_2). WAG operation has been widely applied in enhanced oil recovery since the late 1950s. Inspired by the practice in the oil industry, several investigators have surmised that intermittent injection of CO_2 and water could lead to better CO_2 storage efficiency by reducing the migration of CO_2 plume [5],[7], enhancing residual trapping [8],[9] and accelerating the CO_2 dissolution [10],[11]. Improved (reduced) CO_2-brine mobility ratio and accelerated CO_2 dissolution are the two most important characteristics that motivate the adoption of WAG operation in SAGCS. In multiphase flow, the non-wetting phase to wetting phase mobility ratio is defined as:

$$M = \frac{m_n}{m_w} = \frac{\mu_w \cdot k_{rn}}{\mu_n \cdot k_{rw}} \tag{1}$$

where μ_w is the wetting phase viscosity, k_{rw} is the wetting phase relative permeability, μ_n is the non-wetting phase viscosity, and k_{rn} is the non-wetting phase relative permeability. In the context of SAGCS, the pre-existing brine is considered as the wetting phase and injected supercritical CO_2 is considered as non-wetting phase. If the intermittent CO_2-water injection is treated as a quasi-mixture entering the aquifer, it will effectively bring down the mobility ratio compared to that of pure CO_2 injection. The effective mobility ratio is crucial for SAGCS efficiency for the following two reasons:

1. The mobility ratio determines whether the displacement of the reservoir fluid is stable. If $M < 1$, stable displacement occurs, i.e., the displacement of brine acts in a piston-like fashion; if $M > 1$, unstable displacement occurs, resulting in inefficient displacement of brine due to the formation of water/gas fingers.
2. The mobility ratio determines the speed of buoyancy-driven CO_2 migration. Investigation of the vertical migration of CO_2 plumes in porous media has shown that the front-end speed of a 1-D plume changes as the mobility ratio varies: the CO_2 plume front travels faster with higher mobility ratio and vice versa [5]. Since the buoyancy-driven upward

motion is the main cause of excessive lateral migration of in situ CO_2, it implies that in situ CO_2 will rise and spread more slowly by reducing the mobility ratio, resulting in a smaller environmental footprint.

Another key aspect of WAG operation is the enhanced CO_2 dissolution. In the literature, reservoir engineering techniques of injecting brine into the aquifer after the completion of CO_2 injection for achieving accelerated CO_2 dissolution have been studied by Leonenko and Keith [10]. Orr [8] and Bryant et al. [9] also claimed that CO_2-chasing water injection can expedite the process of residual trapping. Promising results have been obtained from both numerical simulations and feasibility analysis. The fundamental mechanism of accelerating CO_2 dissolution by water injection is enhanced convective mixing of CO_2 and brine/water. Since WAG operation consists of repeated cycles of CO_2-chasing water injection, it is expected that the CO_2 dissolution will be enhanced with the deployment of WAG. Considering these facts, optimal design of WAG operation for SAGCS is investigated below.

4.1.1. Optimization of WAG scheme using GA-TOUGH2

The WAG operation is studied for GCS in various saline aquifers (generic and identified large scale) and for different injection well orientations (vertical and horizontal). First, WAG operation for a generic saline aquifer with generic hydrogeological properties is investigated by considering both the vertical and horizontal injection wells. Vertical injection wells are the most common type of well with mature and economical well completion technology. Nevertheless, SAGCS with horizontal well injection is worth investigating since there are potential benefits of horizontal well injection, as has been noted by and Jikich and Sams [11] and Hassanzadeh et al. [12]. Next, WAG optimization is considered for identified large saline aquifers. The Frio formation and Utsira formation are considered in our study. For these formations, all simulation parameters are obtained from the history-matching simulations described in Chapter titled, "Numerical Simulation of CO2 Sequestration in Large Saline Aquifers".

One complete cycle of CO_2-water injection is identified as a WAG cycle. A complete WAG operation is composed of a series of such basic WAG cycles. For simplicity, it is assumed that WAG cycles are identical to each other. A schematic of the considered WAG operation is shown in Figure 2, with red blocks and blue blocks representing CO_2 injection and water injection respectively. The width of the blocks represents the duration of injection.

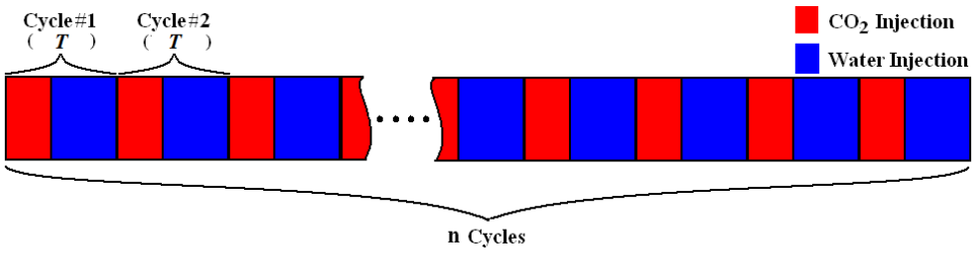

Figure 2. A typical schematic of the WAG operation

http://dx.doi.org/10.5772/57066

A set of four basic variables determines a unique cycle pattern, identified as: CO_2 injection rate I_{CO2}, water injection rate I_{water}, WAG ratio r_{WAG} (the ratio of injected CO_2 mass to injected water mass per cycle), and cycle duration time T. Assuming the duration of CO_2 injection in one WAG cycle as t_{CO2}, the WAG ratio is defined by the following equation (2).

$$r_{WAG} = \frac{m_{CO2}}{m_{water}} = \frac{I_{CO2}t_{CO2}}{I_{water}t_{water}} = \frac{I_{CO2}t_{CO2}}{I_{water}\left(T - t_{CO2}\right)} \tag{2}$$

By rearranging equation (2), the duration of CO_2 injection can be expressed by equation (3).

$$t_{CO2} = \frac{r_{WAG} \cdot I_{water}T}{r_{WAG} \cdot I_{water} + I_{CO2}} \tag{3}$$

Equation (3) suggests that a WAG operation can be uniquely defined if the four basic variables are given. Optimization of these four independent variables becomes a four-dimensional design problem, which can be computationally very expensive. To make the optimization more tractable, WAG cycle duration time T is determined prior to the simulation. It is rather tricky to determine the value of T beforehand. Nasir and Chong [13] have claimed that differences in WAG cycle duration time do not lead to significant differences in recovery efficiency for enhanced oil recovery. However, we have found in our research that WAG cycle duration time can significantly affect the performance of WAG operation under certain conditions. In our simulations/optimizations, we have set T at 30 days, which is an economically feasible and performance-acceptable choice. The effect of WAG cycle duration time on sequestration efficiency is discussed in a later section. With the above simplifications, the number of independent variables that uniquely determines a WAG operation is reduced by two. Since WAG cycle duration time T is pre-determined, any two variables from I_{CO2}, I_{water}, or r_{WAG} can be picked as the basic optimization variables for designing a WAG operation. There is no constraint or preference as to which of these two parameters should be chosen as the optimization design variables. Picking I_{CO2} and I_{water} as the two design variables, the remaining variable r_{WAG} is determined by equation (4).

$$\begin{aligned} r_{WAG} &= \frac{m_{CO2}}{m_{water}} = \frac{M_{CO2}/n}{I_{water}t_{water}} = \frac{M_{CO2}}{nI_{water}\left(T - M_{CO2}/nI_{CO2}\right)} \\ &= \frac{M_{CO2}}{I_{water}\left(nT - M_{CO2}/I_{CO2}\right)} = \frac{M_{CO2}I_{CO2}}{I_{water}\left(I_{CO2}nT - M_{CO2}\right)} \end{aligned} \tag{4}$$

where M_{CO2} is the total amount of CO_2 to be sequestered and n is the total number of WAG cycles.

A given amount of CO_2 to be sequestered is usually known as the sequestration target of a given SAGCS project. A medium-size coal-fired power plant typically generates approximate-

ly 1 million metric of CO_2 annually. For the purpose of our investigation, it is reasonable to assume 50% CCS efficiency, i.e., capture and sequestration of a half million metric tons of CO_2 for a proposed WAG operation in a hypothetical generic aquifer. For WAG operation in identified large aquifers, the target sequestration amount is set identical to that determined for the actual project. Equations (3) and (4) determine the unique WAG patterns. Simulations of non-optimized WAG operations are performed first to demonstrate the reduced CO_2 migration. Recalling that gaseous CO_2 reaches the caprock relatively quickly under buoyancy and then migrates underneath the caprock, it is the radial migration of gaseous CO_2 that causes enormous land use as well as the leakage risk. Therefore, the saturation of gaseous phase CO_2 (SG) directly underneath the caprock, originating from the injection well along the migration direction, should serve as an ideal indicator of storage efficiency. SG is the percentage of void space in the formation occupied by gaseous CO_2; thus it varies from 0 to 1. It becomes greater than zero when CO_2 displacement of brine occurs, and remains zero in CO_2 free zones. Therefore, the maximum migration of in situ CO_2 can be effectively determined by examining the SG profile underneath the caprock. Additionally, cross-sectional SG contours can also indicate the migration and dissolution of in situ CO_2.

4.1.2. WAG injection in a hypothetical generic saline formation with a vertical injection well

A hypothetical generic cylindrical domain with thickness of 100 m is considered as the target aquifer. The radius of the aquifer is set at 3000 m to minimize the influence of the boundary conditions. For generalization purposes, typical hydrogeological properties of deep saline aquifers are applied to the domain. CO_2 and water are injected at the center of the domain by an injection well fully perforating the aquifer. No water pumping is included in the simulation domain, with the assumption that water production is either far away from the storage site or comes from a nearby water reservoir. The WAG operation is assumed to consist of 20 WAG cycles, each lasting for 30 days. The injection operation therefore lasts for 600 days. CO_2 migration is examined 50 years after the inception of injection. Figure 3 shows the computational model and the mesh. Due to symmetry, only a radial slice of the aquifer is modeled. The computational mesh is highly refined near the injection well and near the caprock to accurately capture the migration of in situ CO_2 in those regions.

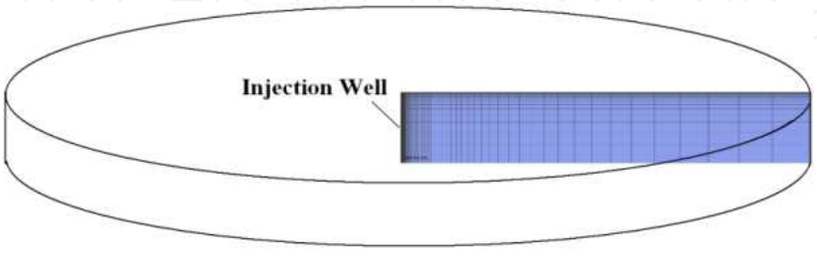

Figure 3. Generic domain for optimization of WAG operation with a vertical injection well

Table 1 summarizes the details of the model geometry, the hydrogeological properties and the simulation parameters.

http://dx.doi.org/10.5772/57066

Permeability	Isotropic, 100 mDarcy
Porosity	0.12
Residual Brine Saturation	0.2
Residual CO_2 Saturation	0.05
Relative Permeability	van Genuchten-Mualem
Capillary Pressure	van Genuchten-Mualem
Initial Conditions	P = 12 MPa, T = 45 °C
Initial CO_2 Mass Fraction	$X_{CO2} = 0$
Initial Salt Mass Fraction	$X_{sm} = 0.15$

Table 1. Hydrogeological properties and initial conditions for the cylindrical domain considered for the optimization study of WAG operation with vertical well injection

The fitness function of the optimization, i.e., the criteria for evaluating the performance of a certain WAG operation, is defined as the ratio of CO_2 migration reduction (with respect to that of CGI operation) to the total amount of water injection. It is mathematically represented by equation (5). This choice of fitness function arises from the consideration of the economic feasibility of implementing the WAG operation, since the transportation and pumping of water is likely to consume additional energy. It is obvious that a tradeoff exists between the water consumption and CO_2 migration reduction. Therefore, it is clear that the WAG operation leading to the maximum value of the fitness function would provide the optimal balance between the plume migration reduction and water requirement.

$$fitness = \frac{R_{CGI} - R_{WAG}}{m_{water}} \tag{5}$$

As mentioned earlier, I_{CO2} and I_{water} have been chosen as the two optimization design variables. The search space is [30 kg/s,100 kg/s] for both I_{CO2} and I_{water}, resulting in the search space for r_{WAG} as [0.19, 1.18]. A post-processing computational module has also been developed for determination of the migration reduction. The design variable values corresponding to optimal WAG operation and the optimal fitness function are determined as $I_{CO2,optimal}$ = 55.26 kg/s, $I_{water,optimal}$ = 39.19 kg/s, $r_{WAG,optimal}$ = 0.567, and $fitness_{optimal}$ = 0.0605 m/10^3 metric tons of water. Correspondingly, the durations of CO_2 and water injection in one WAG cycle can be calculated to be 8.6 and 21.4 days respectively. Thus, in each WAG cycle, CO_2 injection lasts for 8.6 days with an injection rate of 55.26 kg/s before it is cut off; then water injection begins with an injection rate of 39.19 kg/s until the 30-day cycle duration is completed. Identical WAG cycles repeat 20 times to complete the 600-day injection operation. Figure 4 shows the schematic of the optimal WAG operation.

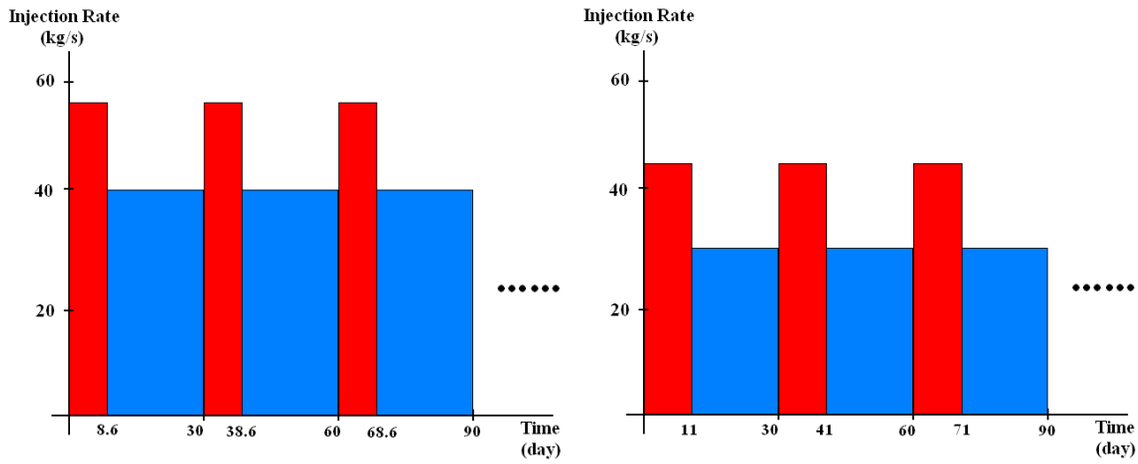

Figure 4. Graph of the optimized WAG operation with vertical well injection

Table 2 summarizes the technical benefits of applying the optimal WAG operation.

		Vertical Injection Well
CGI	CO_2 Radial Migration	1210 m
WAG	CO_2 Radial Reduction	87.66 m
	CO_2 Radial Reduction Ratio	7.24 %
	CO_2 Impact Area Reduction	642308 m^2
	CO_2 Impact Area Reduction Ratio	14%
	Total Water Injection Required	1448600 metric tons

Table 2. Summary of the benefits of implementing optimized WAG operation with vertical injection well

The corresponding CO_2 plume migration under the caprock is compared to the CGI operation in Figure 5. As summarized in Table 2 and shown in Figure 5, a 14% reduction in CO_2 impact area and significantly lowered CO_2 accumulation underneath the caprock can be achieved by replacing the conventional CGI operation with the optimal WAG injection. The cost of such a benefit is the pumping work required to inject 1448600 metric tons of water plus the extra CO_2 pumping work needed due to the increased injection pressure.

4.1.3. WAG injection in a hypothetical generic saline formation with a horizontal injection well

Jikich and Sams [11] and Hassanzadeh et al. [12] have suggested the potential benefits of utilizing horizontal injection wells for SAGCS. It has been claimed that vertical wells provide insufficient injectivity, while horizontal injectors can greatly improve injectivity and storage capacity. Hassanzadeh et al. have also suggested that horizontal injection well can lead to significantly higher CO_2 dissolution rate compared to the vertical injection well when water chasing injection is applied [12]. These suggested benefits of horizontal injection well have motivated us to apply and optimize WAG operation for horizontal well injection. Unlike the perfectly symmetric flow patterns with vertical injection well, a full 3D model is required when

http://dx.doi.org/10.5772/57066

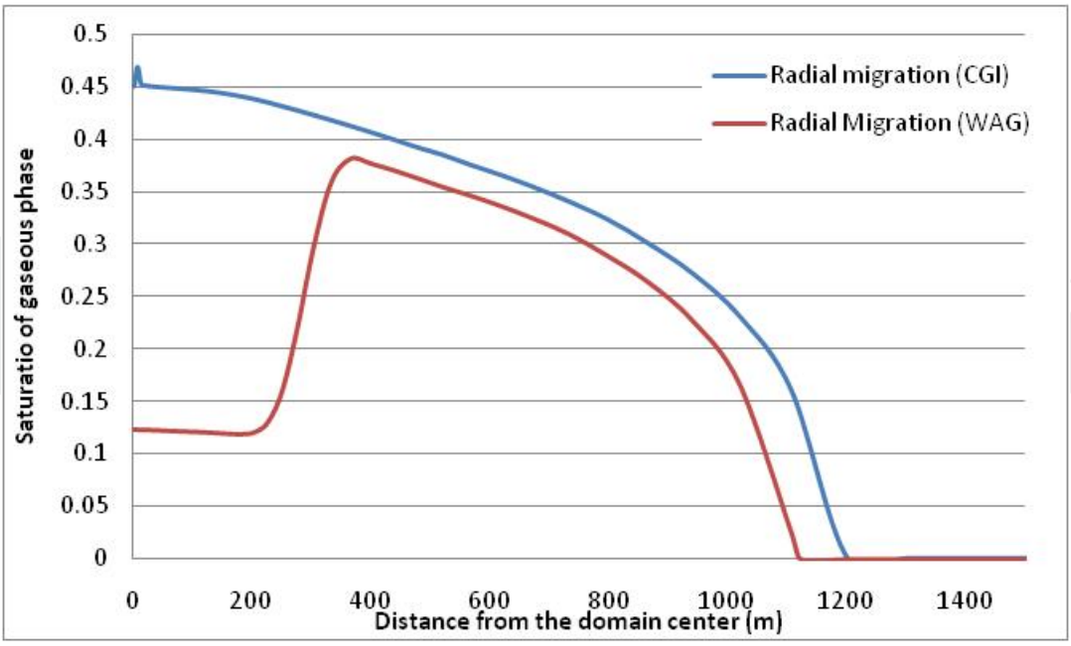

Figure 5. Radial gas saturation comparisons of optimized WAG operation and the non-optimized CGI operation for vertical injection well

horizontal injection well is considered since the flow patterns are no longer symmetric. As a result, the modeling and simulation of the SAGCS with horizontal injection well becomes computationally more intensive and requires higher computational cost. A hypothetical generic aquifer of dimensions 8000 m × 8000 m × 100 m is considered. It is assumed that an 800-m horizontal injection well sits in the middle of the aquifer. Due to symmetry, only a quarter of the domain is modeled, as shown in Figure 6. The modeled computational domain is therefore of the dimensions 4000 m × 4000 m × 100 m with a 400-m horizontal injector sitting in the middle of this domain. All the hydrogeological properties and simulation parameters are the same as used in case of vertical well injection (Table 1). The boundary conditions and the target injection amounts are adjusted for the quarter domain under consideration.

The introduction of horizontal injection well causes uneven CO_2 migration along the two principal axial directions. Since the top-planview of the CO_2 plume is expected to be elliptic instead of circular, it requires modification of the fitness function from the previous one used in the vertical well injection case. For simplicity, the average value of the migration distance along the two principal directions is employed to estimate the fitness function. Therefore, equation (5) is modified as:

$$fitness = \frac{R_{CGI} - R_{WAG}}{m_{water}} = \frac{\left(R_{CGI,x-direction} + R_{CGI,y-direction}\right)/2 - \left(R_{WAG,x-direction} + R_{WAG,y-direction}\right)/2}{m_{water}} \quad (6)$$

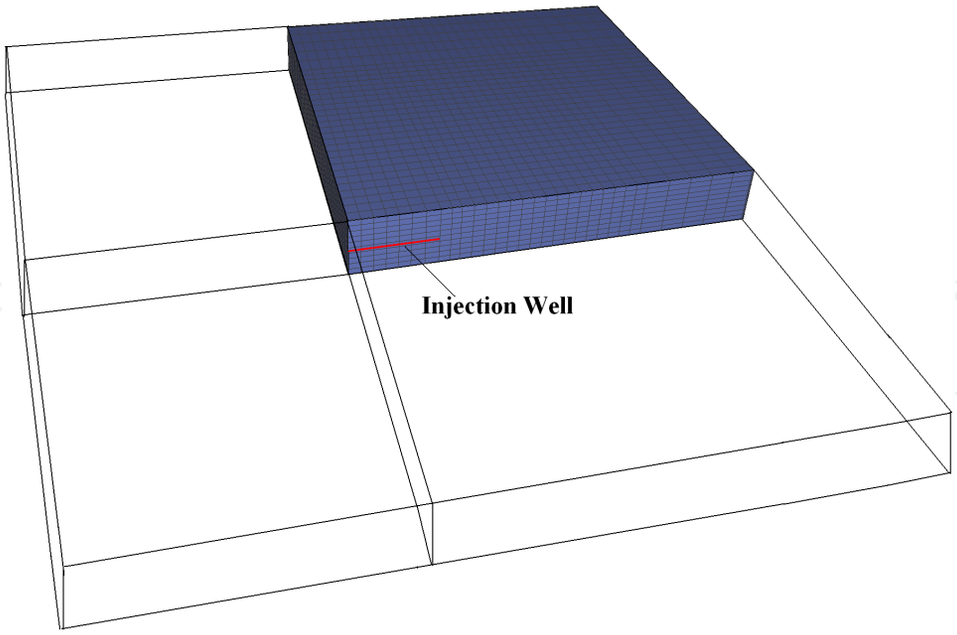

Figure 6. Quarter computational domain for WAG operation with horizontal injection well

where $R_{x\text{-}direction}$ and $R_{y\text{-}direction}$ represent the CO_2 migration distance along the direction of the injection well and in a direction perpendicular to it respectively. Again, I_{CO2} and I_{water} are chosen as the design variables. The search space of I_{CO2} and I_{water} is [20 kg/s, 80 kg/s] and the corresponding search space of r_{WAG} is [0.25, 1.95]. The values of design variables corresponding to optimal WAG operation and the optimal fitness function value are determined as $I_{CO2,optimal}$ = 44.87 kg/s, $I_{water,optimal}$ = 29.59 kg/s, $r_{WAG,optimal}$ = 0.823, and $fitness_{optimal}$ = 0.0718 m/10^3 metric tons of water. Correspondingly, the durations of CO_2 and water injection in one WAG cycle are calculated as 11 and 19 days respectively. Identical WAG cycles are repeated 20 times to complete the entire 600-day operation. Figure 7 shows the optimal WAG operation.

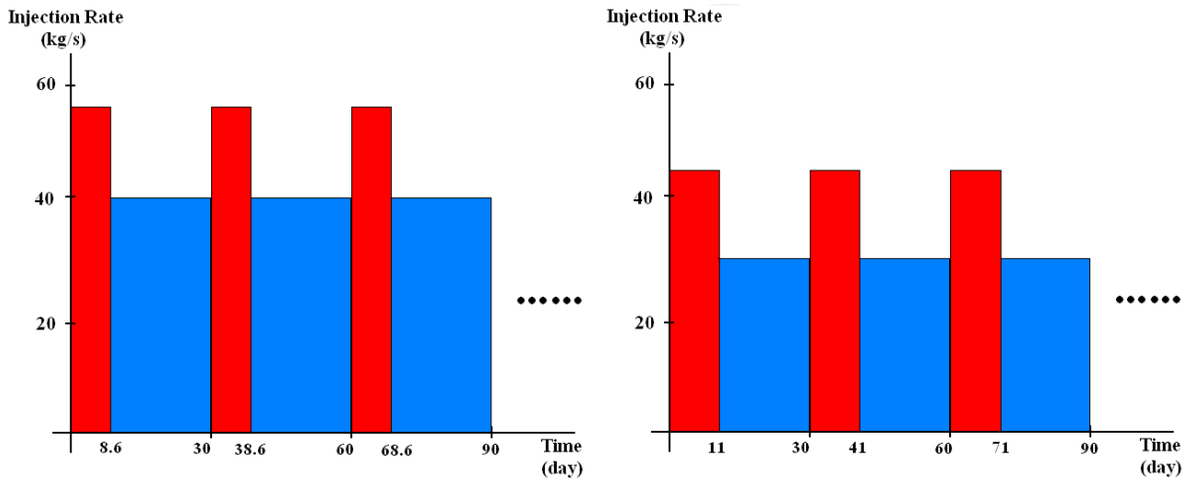

Figure 7. Graph of the optimal WAG operation with horizontal injection well

http://dx.doi.org/10.5772/57066

Table 3 summarizes the technical benefits of applying the optimal WAG operation with horizontal injection well. The corresponding CO_2 plume migration underneath the caprock is compared to that for the CGI operation in Figure 8.

		Horizontal Injection Well
CGI	CO_2 Radial Migration	*x*-direction: 1082.7 m, *y*-direction: 865.7 m
WAG	CO_2 Radial Reduction	*x*-direction: 116.1 m, *y*-direction: 26.9 m
	CO_2 Radial Reduction Ratio	*x*-direction: 10.7 m, *y*-direction: 3.1 m
	CO_2 Impact Area Reduction	397560 m^2
	CO_2 Impact Area Reduction Ratio	14%
	Total Water Injection Required	995635 metric tons

Table 3. Summary of the benefits for implementing optimized WAG operation with horizontal injection well

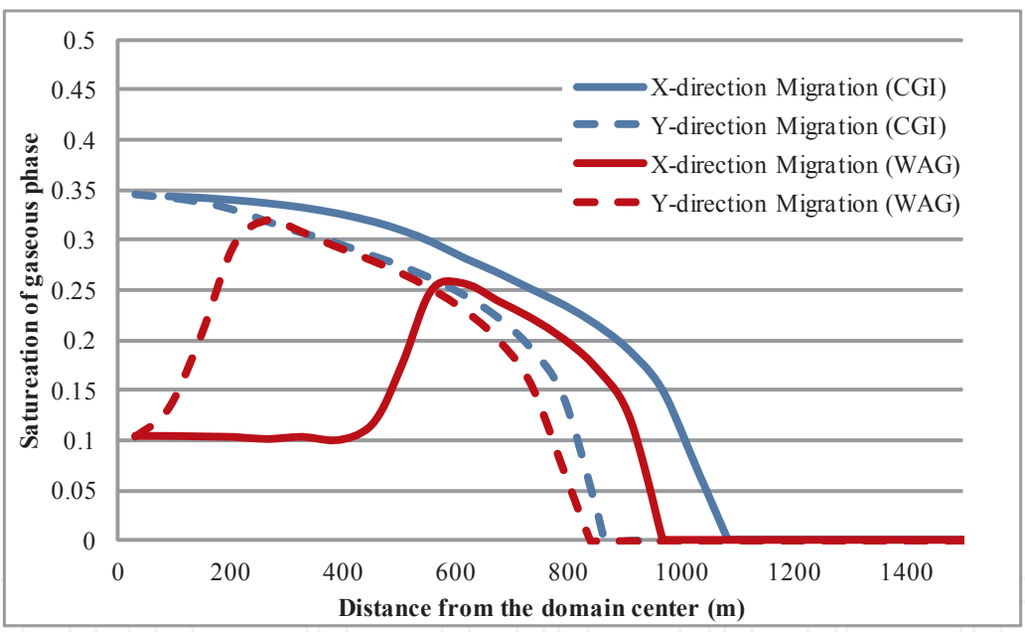

Figure 8. Radial gas saturation comparisons of optimized WAG operation and non-optimized CGI operation using a horizontal injection well

As summarized in Table 3 and shown in Figure 8, a 14% reduction in CO_2 impact area and significantly lowered CO_2 accumulation underneath the caprock can be achieved by replacing the conventional CGI operation with the optimal WAG injection. The cost of such benefits is the pumping work required to inject 995635 metric tons of water plus the extra CO_2 pumping work needed due to the increased injection pressure. These results are qualitatively similar to those obtained for the WAG operation with a vertical injection well. However, the water consumption of the WAG operation with a horizontal injection well is substantially less, implying significantly less energy penalty and improved technical and economic feasibility.

4.1.4. WAG operation with a vertical injection well over an anisotropic saline formation

Actual aquifers are generally heterogeneous in all aspects. It is generally agreed that heterogeneity can cause channeling and fingering of the CO_2 plume, thereby increasing the risk of leakage. It is also claimed that the heterogeneity can lead to locally enhanced trapping [8],[9]. Therefore, heterogeneity of aquifer properties should be taken into account if more realistic simulations with higher accuracy are desired. In section 4.2.3 and section 4.2.4, optimizations of WAG operation were performed for a hypothetical generic saline aquifer with generic hydrogeological properties. The results clearly suggested the potential benefits offered by the WAG technique. However, those simulations did not account for several types of uncertainties in the description of the reservoir conditions, among which heterogeneity is likely to have the greatest effect on the in situ migration of CO_2. In this section, we consider the optimization of WAG operation for an aquifer with anisotropy. Anisotropy of permeability, especially horizontal-to-vertical permeability anisotropy, is the most important property that can have a significant effect on vertical CO_2 migration. According to the laboratory studies of core samples, the horizontal permeability of a saline formation normally is 10~1000 times greater than the vertical permeability. On the other hand, geological stratification such as seen in the Mt. Simon formation also significantly reduces the effective vertical permeability by several orders of magnitude, resulting in drastic anisotropy in the effective permeability.

In this study, we consider the WAG operation with permeability anisotropy for vertical well injection. The model geometry, domain discretization, reservoir conditions, and all other hydrogeological properties are the same as used in the simulation described before in section 4.2.3. A horizontal-to-vertical permeability ratio of 10, i.e., $k_{horizontal}/k_{vertical}$=10, is considered. A quick estimation of the effective permeability of the Utsira formation indicates that setting the permeability ratio at 10 is actually a conservative value, as shown below.

Considering a stratified formation with all layers being horizontal, the directional flow through that formation will be as shown in Figure 9, in which each layer has its unique permeability as k_1, k_2, k_3, and thickness as h_1, h_2, h_3. The total thickness of the stratified formation is H. Flow transportation in the horizontal and vertical directions is considered separately.

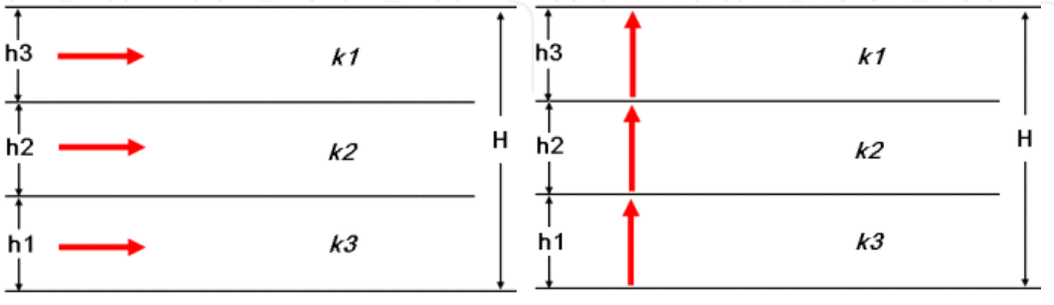

Figure 9. Graph of stratified formation with (a) horizontal flow, and (b) vertical flow

Using the mass conservation law and Darcy's law, equation (7) can be derived to evaluate the equivalent permeability along the two principal directions (horizontal and vertical) as follows.

http://dx.doi.org/10.5772/57066

$$k_{eq,horizontal} = \frac{k_1h_1 + k_2h_2 + k_3h_3}{H} = \frac{\sum kh}{H} \qquad k_{eq,vertical} = \frac{H}{\frac{h_1}{k_1} + \frac{h_2}{k_2} + \frac{h_3}{k_3}} = \frac{H}{\sum \frac{k}{h}} \tag{7}$$

The Utsira formation can be described as a nine-layer structure with sandstone and shale alternatively overlapping each other, as suggested in Audigane et al.'s work [14]. It is assumed that each layer is isotropic in its hydrogeological properties. Detailed descriptions of this nine-layer structure can be found in Chapter titled, "Numerical Simulation of CO2 Sequestration in Large Saline Aquifers". Therefore, the equivalent permeability of the Utsira formation can be evaluated as:

$$\begin{aligned} k_{eq,horizontal} &= \frac{\sum_{i=1}^{9} k_i h_i}{\sum_{i=1}^{9} h_i} = \frac{3\times 70 + 4\times\left(0.01\times 5 + 3\times 25\right)}{70 + 4\times\left(5 + 25\right)} = 2.69 \text{ Darcy} \\ k_{eq,vertical} &= \frac{\sum_{i=1}^{9} h_i}{\sum_{i=1}^{9} \frac{h_i}{k_i}} = \frac{70 + 4\times\left(5 + 25\right)}{\frac{70}{3} + 4\times\left(\frac{5}{0.01} + \frac{25}{3}\right)} = 92.4 \text{ mDarcy} \end{aligned} \tag{8}$$

And the horizontal-to-vertical permeability ratio is obtained as:

$$\frac{k_{eq,horizontal}}{k_{eq,vertical}} = \frac{2.69 \text{ Darcy}}{92.4 \text{ mDarcy}} \approx 29 \tag{9}$$

The simple calculations above give a horizontal-to-vertical permeability anisotropy of 29 for the Utsira formation, i.e., the Utsira formation is 29 times more permeable horizontally than vertically. This demonstrates the existence of permeability anisotropy in actual aquifers, and also assures that assigning a horizontal-vertical permeability ratio of 10 is indeed a conservative choice in our investigation for the design of WAG scheme for an anisotropic aquifer.

Two modifications have been made from the original case of WAG operation study with a vertical injection well described in section 4.2.2. First, horizontal permeability of the formation is increased to 1 Darcy from the original value of 100 mDarcy. Vertical permeability is retained as 100 mDarcy to keep the permeability anisotropy of 10. Another modification is the perforation of the injection well. To take full advantage of the anisotropy, the injection perforation is reduced to one-third of its original length and is placed at the lower aquifer following Bryant's suggestion of "injection low let rise" [9]. Other than these two modifications, all other parameters of the model are retained. Same assumptions for WAG operation, i.e., 20 WAG cycles each lasting 30 days, and identical amount of CO_2 for sequestration, i.e., 0.822 million

metric tons over the 600-day injection, are applied. Slightly different from previous studies of WAG operation over the isotropic formation, CO_2 migration beneath the caprock is examined immediately after the injection ceases. The values of the design variables corresponding to optimal WAG operation and the optimal fitness function value are found as $I_{CO2,optimal}$ = 36.13 kg/s, $I_{water,optimal}$ = 33.65 kg/s, $r_{WAG,optimal}$ = 0.847, and $fitness_{optimal}$ = 0.1438 m/10^3 metric tons of water. Correspondingly, the durations of CO_2 and water injection in one WAG cycle can be calculated to be 13 and 17 days respectively. Identical WAG cycles are repeated 20 times to complete the entire 600-day operation. Figure 10 shows the graph of the optimal WAG operation.

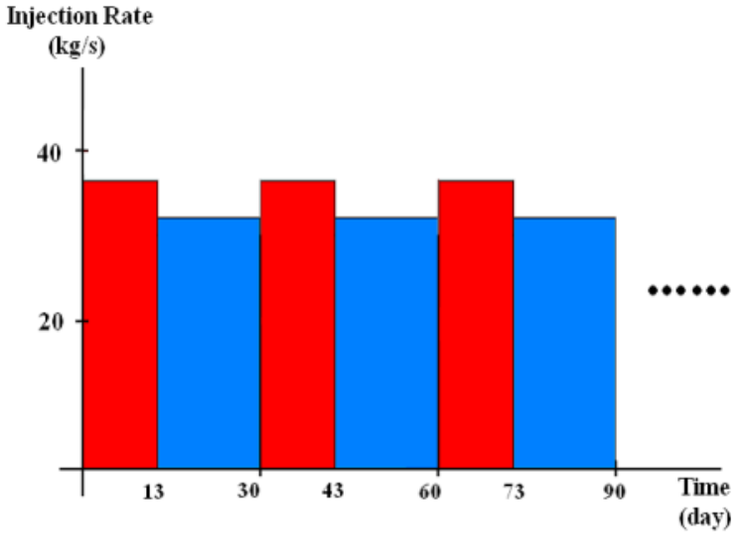

Figure 10. Graph of the optimal WAG operation for anisotropic saline formation

Table 4 summarizes the technical benefits due to adoption of the optimal WAG operation for the anisotropic saline formation.

CO_2 Radial Reduction	140 m
CO_2 Radial Reduction Ratio	32.56 %
CO_2 Impact Area Reduction	316673 m^2
CO_2 Impact Area Reduction Ratio	54.52 %
Total Water Injection Required	973574 metric tons

Table 4. Benefits of implementing the optimized WAG operation in an anisotropic saline aquifer

Figure 11 illustrates the SG curve underneath the caprock of the formation for the optimized WAG operation and that for the CGI operation with CO_2 injection rate of 15.85 kg/s.

As seen from Table 4 and Figure 11, consideration of permeability anisotropy has greatly improved the performance of WAG operation. Under a conservative horizontal-to-vertical permeability ratio of 10, the CO_2 footprint after a 600-day injection program is significantly

http://dx.doi.org/10.5772/57066

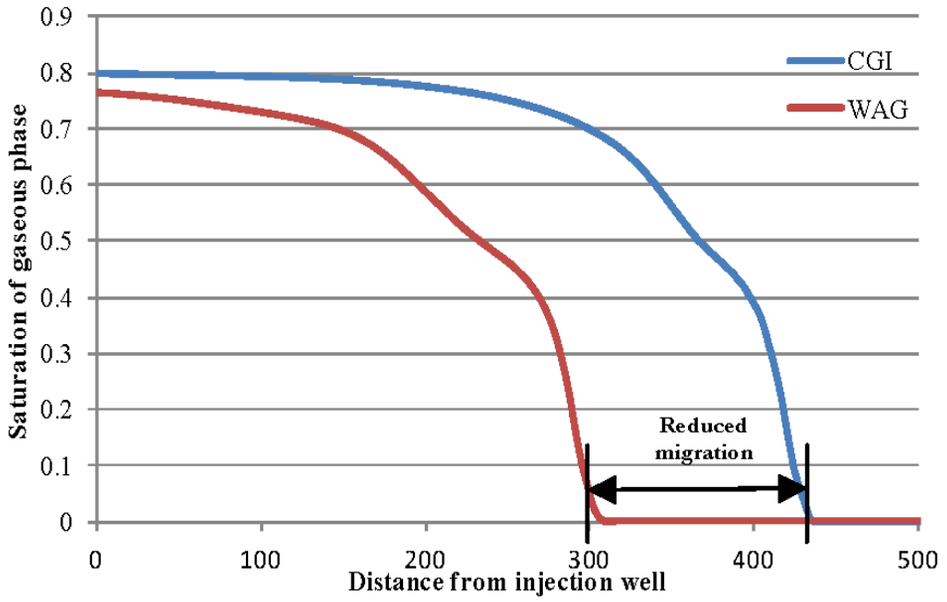

Figure 11. SG underneath the caprock showing migration reduction with optimized WAG operation in an anisotropic saline aquifer

reduced by 54.52%. Recalling the 14% reduction in CO_2 footprint for the isotropic formation, one can draw the conclusion that the anisotropy of formation permeability is an important parameter for high-performance WAG operation. It is also expected that even better performance of WAG operation would be achieved with a higher horizontal-to-vertical permeability ratio. Moreover, the CO_2 injection rate is significantly lower than that for the isotropic formation case. The duration of CO_2 injection in each WAG cycle is increased by about four days to maintain the overall injection amount. The lower injection rate and increased injection duration suggest improved injection conditions such as lower injection pressure.

To have a better illustration of the CO_2 migration reduction, simulations of three other non-optimized injection scenarios were conducted, namely constant-gas-injection with low injection rate (low-CGI), constant-gas-injection with high injection rate (high-CGI), and cyclic CO_2 injection. For the low-CGI case, CO_2 is injected with a constant mass flow rate of 15.85 kg/s for 600 days; for the high-CGI case, CO_2 is injected with a constant mass flow rate of 31.71 kg/s for 300 days; cyclic CO_2 injection is very similar to the optimal WAG injection except that water injection is removed from the operation. Therefore, all three additional cases have an identical amount of injected CO_2 but zero water injection. Comparison of the SG curves of the optimized WAG operation and the three non-optimized injection scenarios are shown in Figure 12 and Figure 13, and summarized in Table 5.

Figure 13 shows SG contours for the optimized WAG and three non-optimized injection scenarios after 600 days of injection at the radial cross-section of the formation.

Table 5 provides detailed comparisons between the optimized WAG operation and three non-optimized injection scenarios. The reduction of in situ CO_2 migration in optimized WAG is prominent.

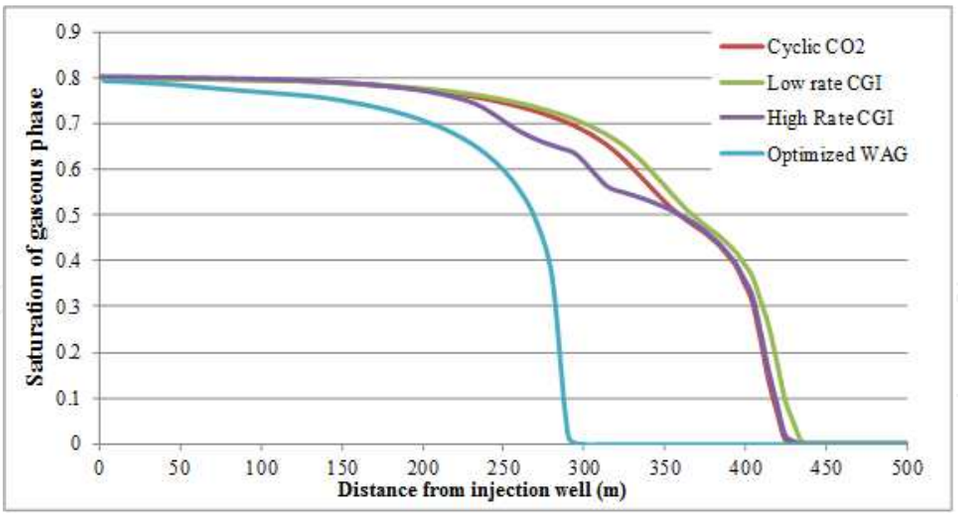

Figure 12. SG underneath the caprock; optimized WAG and non-optimized injection operations in an anisotropic saline aquifer

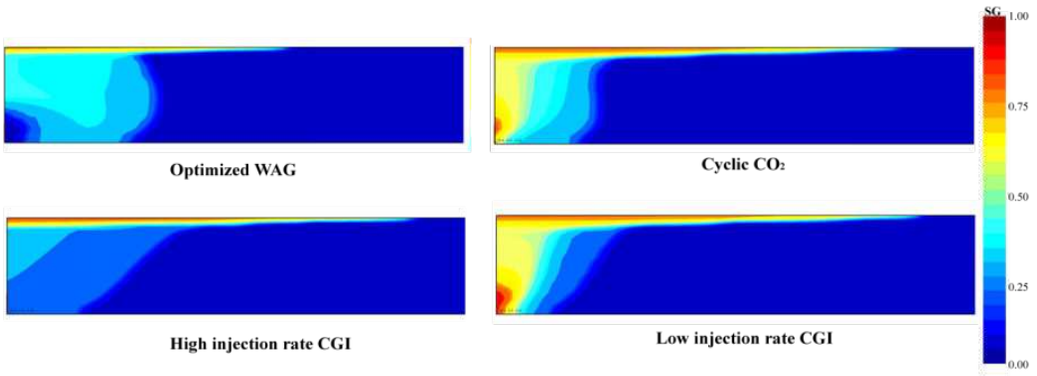

Figure 13. SG contours for optimized WAG and three non-optimized injection operations

Relative to Optimized WAG	Optimized WAG	Cyclic CO_2 Injection	High Rate CGI	Low Rate CGI
CO_2 Plume Migration	290 m	420 m	420 m	430 m
Additional CO_2 Migration	-	130 m	130 m	140 m
Increased Plume Radius	-	44.83 %	44.83 %	48.28 %
Increased Footprint Area	-	109.75 %	109.75 %	119.86 %

Table 5. CO_2 migration comparisons of optimized WAG with three other non-optimized injection scenarios

The results presented above clearly show the benefits of the WAG injection in reducing the in situ CO_2 migration. However, tradeoffs of such benefits need to be carefully considered for the safety and feasibility of SAGCS utilizing WAG operation. One of the most critical operational parameters of SAGCS is the pressure. The bottom line is that injection-induced pressure must not exceed the formation's fracture pressure under any circumstance. In practice, injection

http://dx.doi.org/10.5772/57066

pressure is closely monitored and it is common to temporarily reduce the injection rate in order to reduce overly high injection pressure. Figure 14 shows the injection pressure (average value of the injection well) under the optimized WAG operation. According to our investigation, the optimized WAG operation causes the injection pressure to oscillate as the CO_2 injection and water injection alternate. Considering the peak pressure, an 8% increase of reservoir pressure from its hydrostatic condition can be noticed near the injection well under the optimized WAG operation. On the other hand, a maximum of 2% increase in reservoir pressure is induced in the three non-optimized injection scenarios. Therefore, one can draw the conclusion that harsher injection conditions are inevitable with WAG operations. However, the induced pressure elevation by WAG operation could be moderate enough not to pose significant concerns. It should also be pointed out that reservoir pressure response to the injection of CO_2 and water is very sensitive to the hydrogeological properties of the formation, such as porosity and permeability. Pressure analysis should be performed on a case-by-case basis for different saline formations to ensure the feasibility and safety of WAG operation.

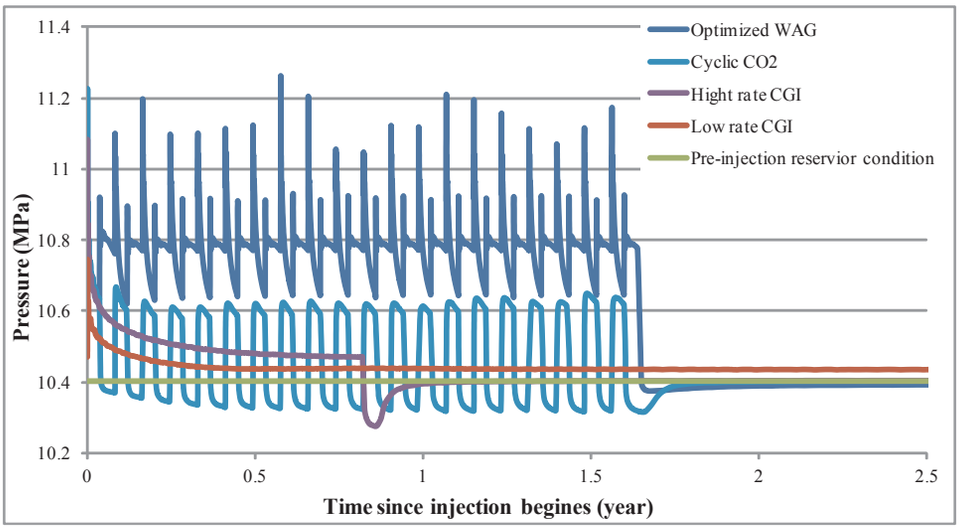

Figure 14. Reservoir pressure response of optimized WAG and three non-optimized injection schemes

With the success of CO_2 migration reduction using WAG operation for generic saline aquifers, we decided to test the performance of WAG operation in numerical models with hydrogeological properties of real large-scale aquifers. For this purpose, we consider the three representative models of identified large saline formations described in Chapter titled, "Numerical Simulation of CO2 Sequestration in Large Saline Aquifers" for numerical implementation and optimization of WAG operation. These three models are the one established for the Frio pilot project, the generalized cylindrical Utsira formation model, and a newly established cylindrical Utsira Layer #9 model. The Frio model represents the saline formation of relatively small thickness but with significant geological slope. The generalized Utsira model represents the saline formation with relatively large thickness and stratified hydrogeology. The cylindrical Utsira Layer #9 model is a good representative of saline formation with relatively small thickness and anisotropic hydrogeology.

4.1.5. WAG operation for generalized Utsira formation model

In contrast to the Frio formation, the generalized Utsira model for SAGCS has insignificant geological slope and relatively large thickness. Recalling the simulation studies of the Sleipner SAGCS project in Chapter titled, "Numerical Simulation of CO2 Sequestration in Large Saline Aquifers", the Utsira formation is a layered formation with about 200 m in thickness without evidence of any significant geological slope. Therefore, the cylindrical model of the layered Utsira formation presented in Chapter titled, "Numerical Simulation of CO2 Sequestration in Large Saline Aquifers" is used to study the WAG operations. All hydrogeological properties and numerical conditions used before as described in Chapter titled, "Numerical Simulation of CO2 Sequestration in Large Saline Aquifers" are retained, including the amount of CO_2 injection at a rate of 1 million metric tons per year. The conventional CGI operation used in the Chapter titled, "Numerical Simulation of CO2 Sequestration in Large Saline Aquifers" is replaced by the WAG operation. Reduction in radial CO_2 migration under the caprock is examined as the optimization criterion for five years of injection. The generalized Utsira formation model consists of nine alternating shale and sandstone layers, and the injection takes place at the middle of the bottom sandstone layer. The assumption of 30-day WAG cycle duration is retained, as employed in all the previous simulations discussed in sections 4.2.2 – 4.2.4. The WAG operation lasts for five years, during which 1 million metric tons of CO_2 is injected annually. The radial migration of CO_2 in the topmost sandstone layer is examined after two, three, and five years of injection. The values of the design variables corresponding to optimal WAG operation and the optimal fitness function value are found as $I_{CO2,optimal} = 95.72$ kg/s, $I_{water,optimal} = 75.32$ kg/s, $r_{WAG,optimal} = 0.64$, and $fitness_{optimal} = 0.0251$ m/10^3 metric tons of water. Correspondingly, the durations of CO_2 and water injection in one WAG cycle can be calculated as 10 and 20 days respectively. Identical WAG cycles are repeated 20 times to complete the entire five-year operation. Figure 15 shows the graph of the optimal WAG operation for the generalized Utsira formation model.

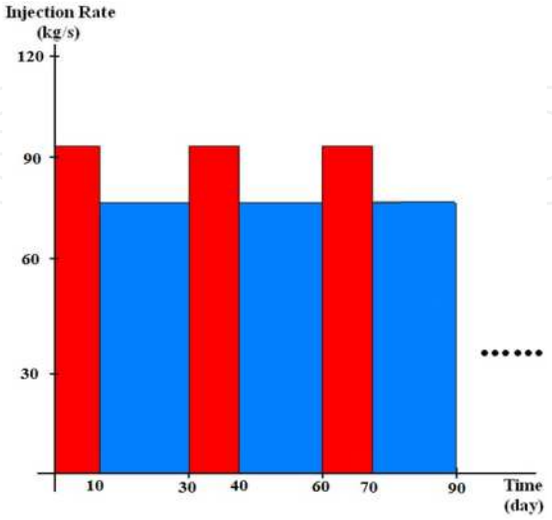

Figure 15. Graph of optimized WAG operation for Utsira formation

http://dx.doi.org/10.5772/57066

Figure 16 shows the CO_2 migration underneath the caprock at the second, third and fifth year for optimized WAG and conventional CGI operations. The reduction in radial CO_2 migration is prominent for the WAG operation.

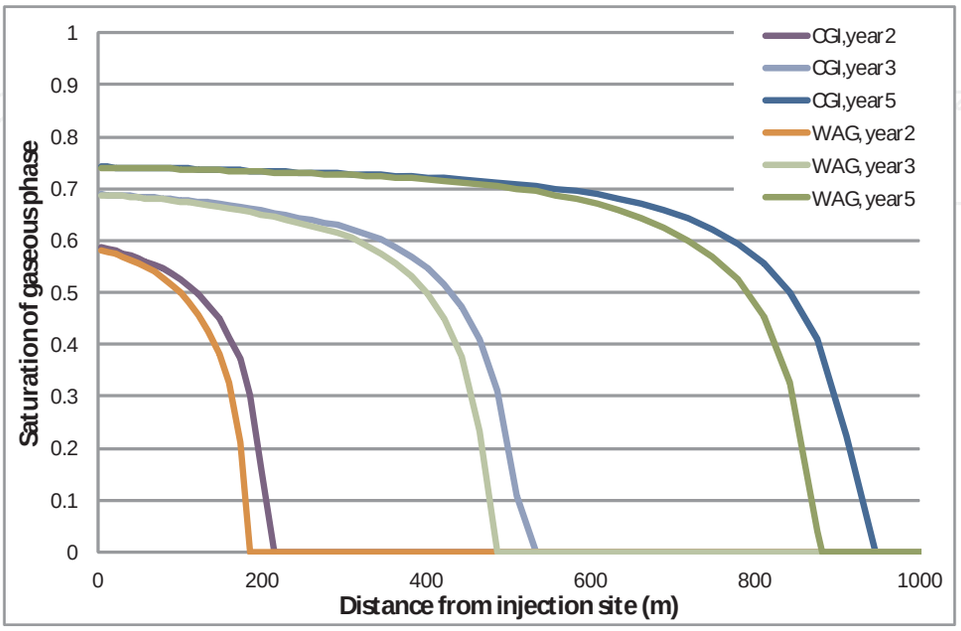

Figure 16. SG underneath the caprock showing plume reduction with optimized WAG operation for Utsira formation SAGCS

Table 6 summarizes the benefits of adopting the optimized WAG operation for the generalized Utsira formation model.

CGI	CO_2 Radial Migration	946.7 m
	Dissolution	16.89 %
WAG	CO_2 Radial Reduction	65.2 m
	CO_2 Radial Reduction Ratio	6.89 %
	CO_2 Impact Area Reduction	372,095 m^2
	CO_2 Impact Area Reduction Ratio	13.23 %
	Total Water Injection Required	1.5625 million metric tons annually
	Dissolution	23.43 %

Table 6. Benefits of implementing the optimized WAG operation for Utsira formation SAGCS

As seen from Figure 16 and Table 6, CO_2 migration under the caprock in the generalized Utsira formation has been significantly reduced by the WAG operation. Compared to the case of the Frio formation, a higher optimization fitness value for the Utsira formation model means more

effective WAG operation. The time-elapsed CO_2 migration recorded in Figure 16 provides clear evidence that reduction in CO_2 migration can be observed as early as two years after injection. More importantly, it can also be seen that migration reduction in later years tends to be greater than that in earlier years, suggesting the development of greater reduction in CO_2 migration as injection proceeds. This is an encouraging result considering the decade-long lifespan of SAGCS projects. It is also useful to investigate how the layered structure of the formation affects the performance of the WAG operation. A closer look at the in situ CO_2 migration for conventional CGI operation (shown in Figure 17) and optimized WAG operation (shown in Figure 18) provides information on the effect of a layered structure on conventional CGI and optimal WG operation.

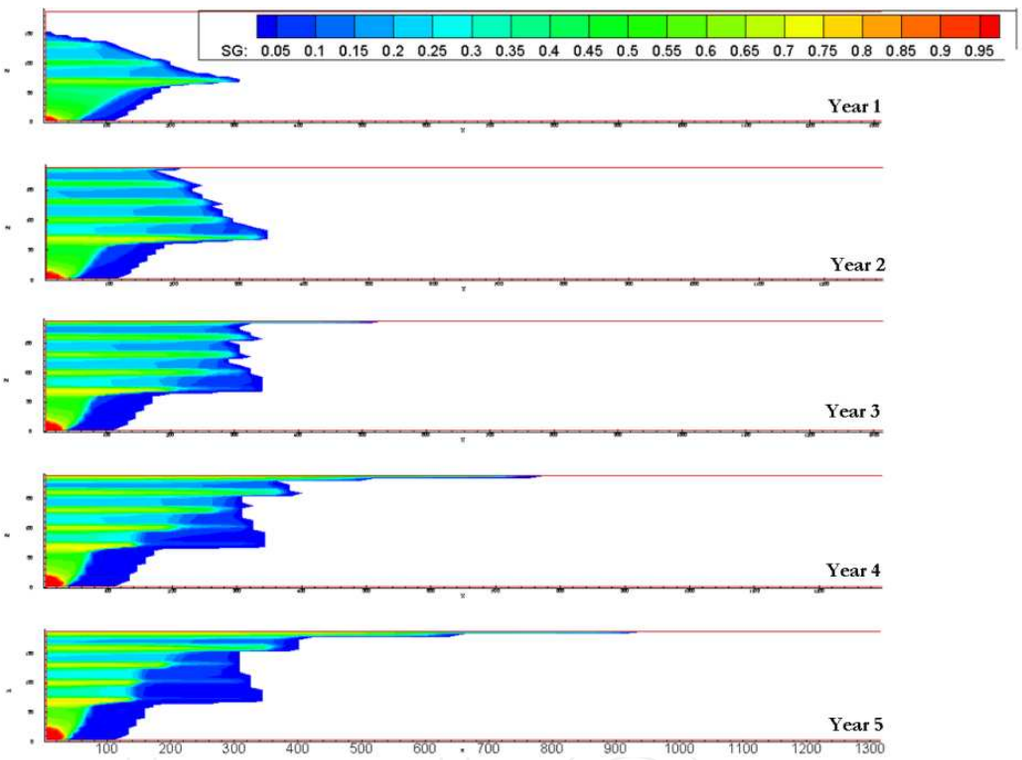

Figure 17. CO_2 plume migration during the first 5 years of CGI operation for the Utsira formation

The generalized Utsira formation model has an equivalent horizontal-to-vertical permeability ratio of 29 according to the calculation presented in Section 4.2.4. The simulations presented in Section 4.2.3 showed great improvement in WAG performance due to the anisotropic permeability. Similar conclusion can be also drawn from the simulation results presented in this section. Comparing Figure 17 and Figure 18 side by side, it can be seen that in situ CO_2 migration has been significantly reduced by the WAG operation, under which the displacement of brine in the lower sandstone layer becomes more stable. Storage efficiency increases under such scenario since more pore-space can now be occupied by supercritical CO_2. Additionally, storage safety is also improved due to the lowered concentration of supercritical CO_2.

http://dx.doi.org/10.5772/57066

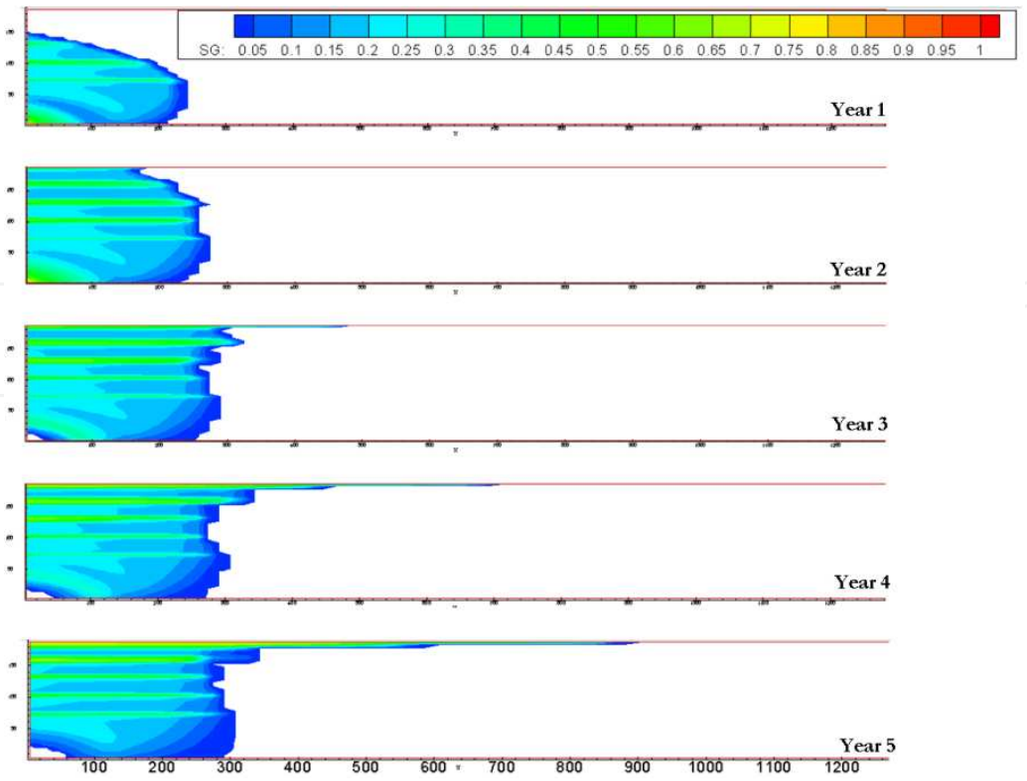

Figure 18. CO_2 plume migration during the first 5 years of optimized WAG operation for the Utsira formation

However, the fitness function value for the layered Utsira formation is not as satisfactory as that for the generic anisotropic aquifer (0.0251 versus 0.1438), although the former case has a higher permeability ratio. Two possible explanations are proposed for these results. First, the upward migration (as well as the resulting radial migration) of in situ CO_2 has already been significantly retarded by the secondary-sealing effect introduced by the layered structure of the formation. Recalling previous analysis, it can be seen that the migration reduction mechanism is similar for both WAG operation and the secondary sealing effect. Secondly, the CO_2 injection rate is set at 1 million metric tons annually for the layered Utsira formation, while it was 0.5 million metric tons annually for the generic anisotropic aquifer. This doubling of CO_2 injection rate for the Utsira formation effectively speeds up the upward migration of in situ CO_2. However, as has been previously discussed, CO_2-water interaction has to take place before the slug reaches the caprock to ensure the superior performance of WAG operation. It is therefore the enhanced upward migration of CO_2 together with the secondary sealing effect that make the WAG operation less satisfactory when applied to the generalized layered Utsira formation model compared to the WAG operation for the generic anisotropic aquifer.

4.1.6. WAG operation for Utsira Layer #9 model

The topmost sandstone layer (Layer #9) of the Utsira formation as presented in Chapter titled, "Numerical Simulation of CO2 Sequestration in Large Saline Aquifers" can serve as another excellent candidate to investigate WAG operation due to its well-understood hydrogeological properties. A cylindrical domain with the average thickness of the Utsira Layer #9 is modeled,

which possesses identical characteristics of the detailed 3D Utsira Layer #9 model (from Chapter titled, "Numerical Simulation of CO2 Sequestration in Large Saline Aquifers") except for the absence of 3D topography. Although topographical details can be important in determining the accurate migration of in situ CO_2, such a simplification without compromising accuracy is necessary to analyze the effectiveness of WAG operation on CO_2 migration without incurring excessive computational cost.

The geometric and hydrogeological characteristics of the simplified Utsira Layer #9 model can be summarized as follows. We consider a cylindrical domain with thickness of 35 m with horizontal flat caprock. All hydrogeological properties are retained from the detailed 3D Utsira Layer #9 model described in the previous section, the most important being the horizontal-to-vertical permeability ratio of 10. CGI operation with nine-year average CO_2 injection rate of 2.7 kg/s is considered as the baseline case for comparison. The effect of WAG cycle durations on CO_2 migration is investigated for this relatively thin formation. The 30-day, 15-day, and 5-day WAG cycle durations are considered for the WAG optimization design. Our computations show that for the simplified Utsira Layer #9 model, only the WAG operation with 5-day cycle leads to noticeable migration reduction. Therefore, all results given below are for 5-day WAG cycle. The values of design variables corresponding to optimal WAG operation and the optimal fitness function value are found as $I_{CO2,optimal} = 11.56$ kg/s, $I_{water,optimal} = 7.62$ kg/s, $r_{WAG,optimal} = 0.646$, and $fitness_{optimal} = 0.506$ m/10^3 metric tons of water. Correspondingly, the durations of CO_2 and water injection in one WAG cycle can be calculated as 11 and 19 days, respectively. Identical WAG cycles are repeated 20 times to complete a two-year operation. Figure 19 shows the graph of optimized WAG operation for the simplified Utsira Layer #9 model with 5-day WAG cycle duration.

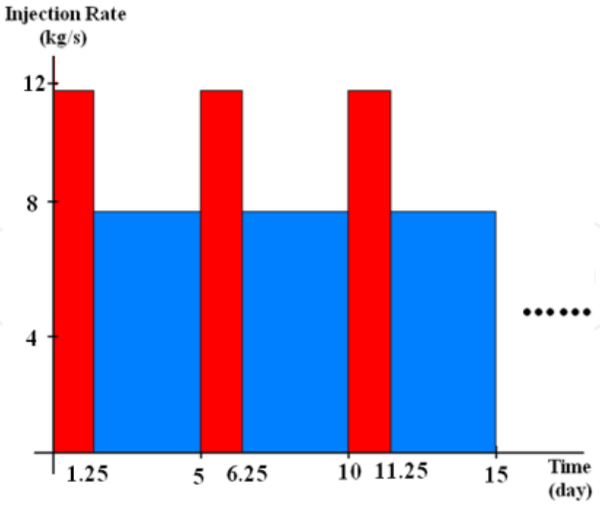

Figure 19. Graph of optimized WAG operation for Utsira Layer #9 model

Figure 20 shows the CO_2 migration underneath the caprock after two years of conventional CGI and optimized WAG operation. The reduction in radial CO_2 migration is significant for WAG operation.

http://dx.doi.org/10.5772/57066

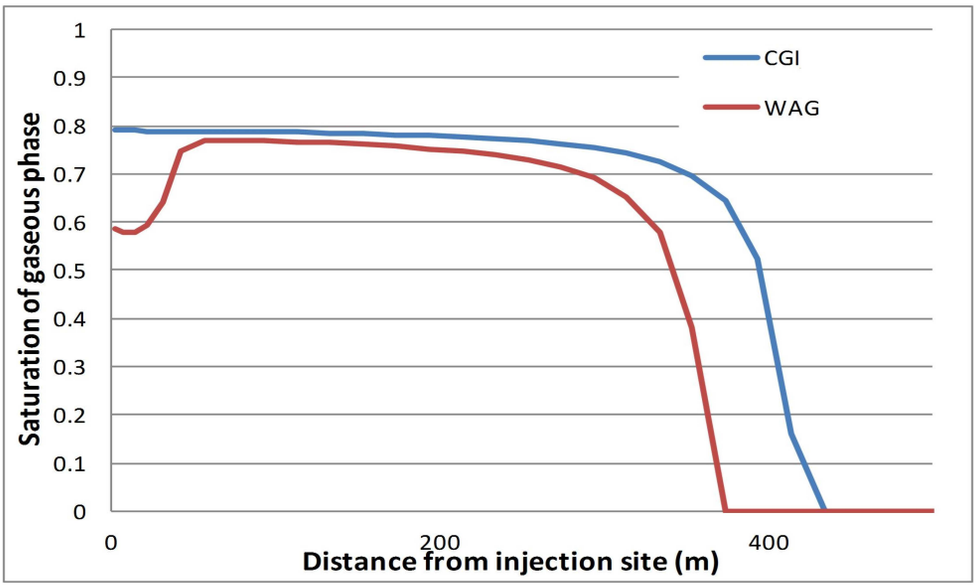

Figure 20. SG underneath the caprock showing plume reduction with optimized WAG injection for Utsira Layer #9 model

Table 7 summarizes the benefits of adopting the optimized WAG injection for the simplified Utsira Layer #9 model.

As seen from Figure 20 and Table 7, significant reduction in CO_2 migration has been achieved after only two years of WAG operation. Additionally, CO_2 dissolution is also significantly enhanced from about 9% to 22% of the total injected CO_2. More importantly, the results reveal the strong relationship between WAG cycle duration and the reservoir thickness regarding the performance of WAG operation. Surprisingly, our simulation results show that the 30-day cycle WAG operation actually "enhances" (not "reduces") the lateral migration of the CO_2 plume. Such a situation can be slightly mitigated when the 15-day WAG cycle duration is applied. However, no noticeable migration reduction is achieved. Considering all three cases of WAG operation for the identified formations, it appears that the aquifer thickness and WAG cycle duration are critical factors affecting the performance of a WAG operation. When the aquifer is thin, it takes less time for the CO_2 to reach the caprock. The assumption of treating alternative water and CO_2 slugs as a quasi-mixture is only valid when injected CO_2 interacts with the chasing water before it reaches the caprock. Failing to fulfill this requirement leads to poor WAG performance. It is the reservoir thickness and WAG cycle duration that determine the validity of quasi-mixture assumption for a given aquifer. Longer WAG cycle duration requires larger reservoir thickness and vice versa. Our simulations show that a minimum reservoir thickness may exist for a given WAG cycle duration under which the quasi-mixture assumption is valid and vice versa. This minimum thickness requirement may ultimately determine the technical feasibility of a WAG operation for an aquifer for achieving any reduction in CO_2 migration. Following this rationale, the success of WAG operation with 5-day cycle duration and its failure with the 15-day and 30-day cycle durations can be explained for Utsira Layer #9 model. This also implies that the CO_2 injected at the bottom of Layer #9

CGI	CO_2 Radial Migration	423 m
	Dissolution	8.97 %
WAG	CO_2 Radial Reduction	49 m
	CO_2 Radial Reduction Ratio	11.58 %
	CO_2 Impact Area Reduction	122689 m^2
	CO_2 Impact Area Reduction Ratio	21.83 %
	Total Water Injection Required	231916 metric tons
	Dissolution	23.02 %

Table 7. Benefits of optimized WAG operation for the Utsira Layer #9 model

reaches the caprock between 5 to 30 days (more likely in approximately 15 days since minor reduction in plume can be observed in this case) with the given reservoir hydrogeological properties and injection parameters.

With the simulation and optimization of WAG operation for the generalized Utsira formation and Utsira Layer #9 model, one can draw the conclusion that the WAG operation certainly holds technical promise to retard the spread of gaseous CO_2 in actual large-scale saline aquifers. It is also obvious from the results that the timeframe of in situ CO_2-water mixing versus the chosen WAG cycle duration are important considerations that must be carefully determined to assure improved reservoir performance from implementation of WAG operation. Various geological factors of the formation, such as geological slope and reservoir thickness, can contribute to insufficient mixing and thus compromise the performance of the WAG operation. Therefore, the operational parameters of WAG operation need to be designed on a case-by-case basis to achieve optimal performance.

4.1.7. Sensitivity of WAG operational parameters

In previous sections, it has been shown that the performance of WAG operation varies depending on the aquifer's geometric and hydrogeological parameters. It is therefore beneficial to look into the effect of various operational parameters on the performance of WAG operation. If the total amount of CO_2 for sequestration is given, any three out of the four operational parameters, namely the CO_2 injection rate (I_{CO2}), the water injection rate (I_{water}), the WAG ratio (r_{WAG}), and the WAG cycle duration (t_{WAG}), determine a unique WAG operation pattern. Using the case of generic anisotropic saline formation for SAGCS described in section 4.2.4, the effect of WAG operational parameters on the performance of WAG operation is investigated. The optimized case presented in section 4.2.4 is used as the baseline case. The CO_2 injection rate (I_{CO2}), water injection rate (I_{water}), and cycle duration (t_{WAG}) are chosen as the WAG operational parameters. Four additional cases are considered, the results of which are summarized in Table 8.

http://dx.doi.org/10.5772/57066

	I_{CO2} (kg/s)	I_{water} (kg/s)	Cycle Duration (day)	r_{WAG}
Baseline Case	36.13	33.35	30	0.847
Variation #1	50	33.35	30	0.697
Variation #2	36.13	50	30	0.565
Variation #3	36.13	33.35	15	0.847
Variation #4	36.13	33.35	50	0.847

Table 8. Various simulations used in the sensitivity study of WAG operation to its operational parameters

The following figures present radial cross-sectional views showing the migration of in situ CO_2 under the above four WAG cases of Table 8. Since all these cases are small variations from the optimal WAG baseline case, they all show significant reduction in CO_2 migration compared to the CGI case. However, the performance of WAG operation (fitness function), which is defined as plume reduction per unit amount of water injection, differs greatly from one case to another. Figure 21 shows the in situ CO_2 distribution in the reservoir for the optimized WAG operation and its variation #1 (with higher CO_2 injection rate compared to the baseline case).

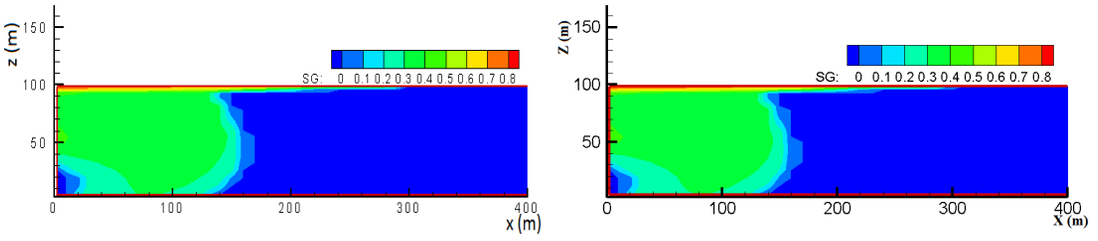

Figure 21. CO_2 distribution in the reservoir (left: optimized WAG; right: WAG with variation #1)

Figure 22 shows the in situ CO_2 distribution in the reservoir for the optimized WAG operation and its variation #2 (with higher water injection rate compared to the baseline case).

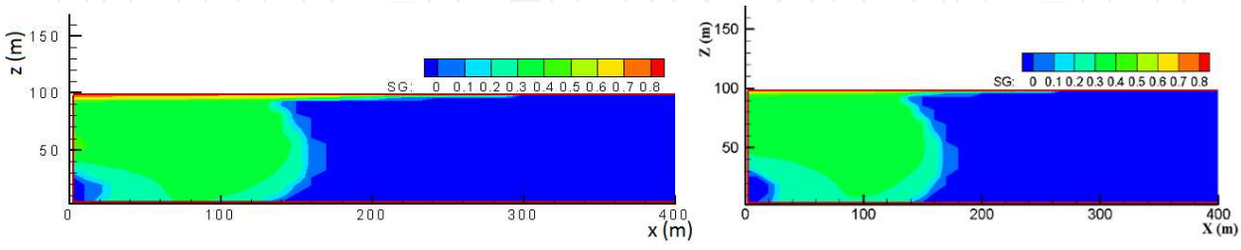

Figure 22. CO_2 distribution in the reservoir (left: optimized WAG; right: WAG with variation #2)

Figure 23 shows the in situ CO_2 distribution in the reservoir for variation #3 and variation #4 (with shorter and longer WAG cycle duration respectively compared to the baseline case).

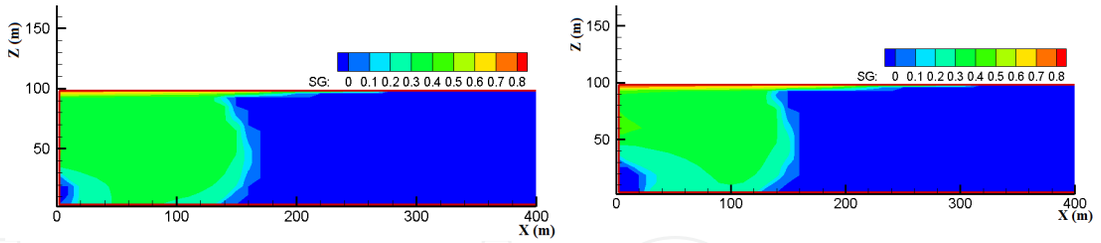

Figure 23. CO_2 distribution in the reservoir (left: WAG with variation #3; right: WAG with variation #4)

Since the lateral extent of the CO_2 plume is determined by the gaseous phase concentration beneath the caprock, its saturation is examined for the original optimized WAG operation and its four variations, as shown in Figure 24.

Table 9 shows the relative performance of the original optimized WAG operation and its four variations.

The results from the above sensitivity analysis are very informative. The following conclusions can be reached. First, none of the four additional cases with slight variations in WAG operational parameters led to higher fitness function value than the optimized baseline case. This result further validates the optimization capability of GA-TOUGH2. Second, CO_2 migration reduction is obtained in all the four cases. Variation case #2 and #4 even achieve greater reduction in migration compared to the baseline case. However, cases with greater migration reduction may not be desirable because the energy penalty (additional water requirement) is more severe for these cases. Third, the crucial role of WAG cycle duration on its performance is also evident. It is clear that the shorter WAG cycle duration is preferable for efficient WAG operation due to the resulting enhanced mixing of CO_2 and water. However, the frequent switching between CO_2 and water injection can be limited by the existing technology barriers.

5. Optimal pressure management

There are two reasons that make the injection pressure one of the most important operational parameters for the success of SAGCS. One is the well injectivity, which determines the total amount of CO_2 that can be injected in a given amount of time, and the other is the safety constraint on injection pressure, which should not exceed the formation's fracture pressure. In petroleum engineering, injectivity of an injection well is defined as the net fluid flow delivered per unit pressure differential between the mean injection pressure and the mean formation pressure. The definition of injectivity is given by equation (10) below.

$$injectivity = \frac{Q_{CO2}}{p_{\text{injection}} - p_{reservior}} \tag{10}$$

http://dx.doi.org/10.5772/57066

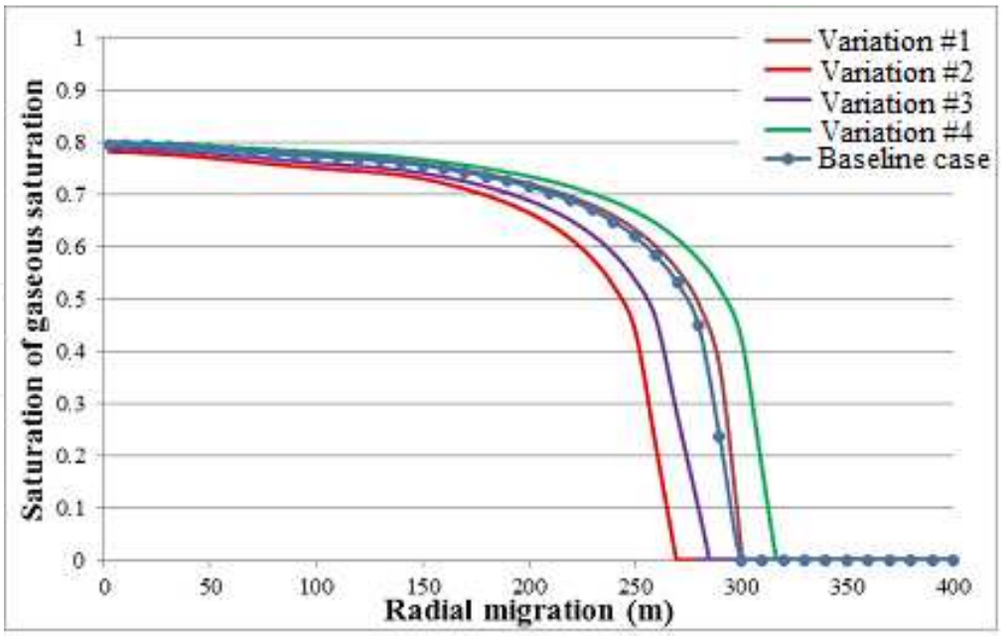

Figure 24. SG underneath the caprock, original optimized WAG operation and its four variations

	Baseline Case	Variation #1	Variation #2	Variation #3	Variation #4
Total CO_2 Injection (kg)	821917	821917	821917	821917	821917
Total Water Injection (kg)	973574	1179222	1454722	973574	973574
WAG ratio	0.847	0.697	0.565	0.847	0.847
Maximum Migration (m)	290	301	270	280	317
Migration Reduction (m)	140	129	160	150	113
Fitness (m/10^3 metric tons water)	0.1438	0.1096	0.1103	0.1545	0.1166

Table 9. Performance of the original optimized WAG operation and its variations

where Q_{CO2} is the injection mass rate and $p_{injection}$ is the injection pressure. The injectivity measure indicates the ability of an injection well to deliver supercritical CO_2 into the aquifer. The injection pressure response for a given SAGCS operation can be analyzed as follows. Applying Darcy's law to the region adjacent to the injection well, the achievable CO_2 injection mass rate Q_{CO2} is proportional to the product of the relative permeability $k_{r,g}$ of CO_2 and the pressure gradient near the injection well Δp. For two-phase flow of supercritical CO_2 and brine, $k_{r,g}$ is inversely proportional to the saturation of brine S_b. At an early stage of CO_2 injection, the pore space near the injection well is primarily occupied by the brine, which means high S_b in the adjacent region of the injection well. As a direct consequence, $k_{r,g}$ is relatively low, which results in considerable difficulty to displace brine by injecting CO_2. A direct indicator of this difficulty is the significant elevation of injection pressure, or in other words, very low injectivity. However, CO_2 injectivity does not remain unchanged. As injection continues, more brine is displaced from the pore space adjacent to the injection well, which effectively lowers S_b.

Simultaneously, $k_{r,g}$ increases. The increased $k_{r,g}$ at intermediate and later stages of CO_2 injection results in improvement of CO_2 injectivity. Therefore, if the injection rate is assumed constant, one can draw the conclusion that at the beginning of injection, high injection pressure is required to overcome the low effective permeability of CO_2. However, as more brine is displaced, injection pressure gradually drops because the permeability of CO_2 increases. Figure 25 schematically shows the effect of injection rate on injection pressure.

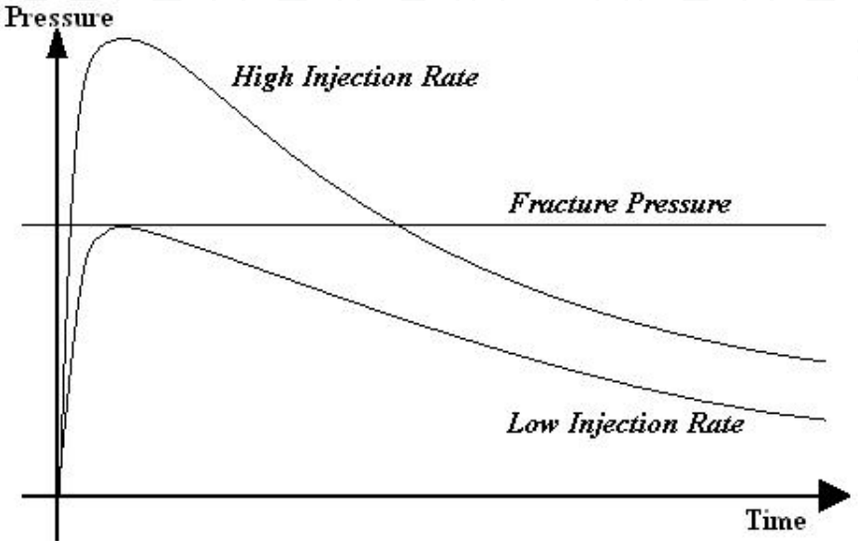

Figure 25. Graph of injection pressure response with time under various CO_2 injection rates

Intuitively, high injection rate is always preferred, since it can lead to more mass injection within a given time. However, a higher injection rate requires greater injection pressure. Regardless of the pumping capacity of the available injection equipment to provide the needed injection pressure, a critical constraint on allowable injection pressure exists. Like all mechanical structures, geological formations can also bear only a certain level of maximum stress while maintaining their integrity. They fracture when excessive stress is applied. Fractures in a formation can serve as pathways for the in situ mobile CO_2 to migrate to shallower aquifers and even all the way to the surface. The leakage of CO_2 through geological fractures is potentially threatening to the ecosystem near the storage site, so needless to say it will also significantly compromise its storage efficiency. Therefore, every attempt should be made to ensure the integrity of the formation, i.e., under no circumstance should the injection pressure exceed the formation's fracture pressure. Since the fracture pressure is an intrinsic property of the formation, it is likely to remain constant during the injection phase of SAGCS, shown by the horizontal line in Figure 25. Considering the injection pressure response under CGI operation and the fracture pressure guideline, Figure 25 reveals a crucial issue that must be addressed. If CO_2 is pumped into the aquifer with a relatively high injection rate (following the "High Injection Rate" scenario in Figure 25), the excessive pressure elevation at the early stage of injection can easily jeopardize the integrity of the formation; on the other hand, if CO_2 is pumped with a relatively low injection rate to ensure the formation's integrity, the injection will become inefficient at the intermediate and late stage since more CO_2 injection

http://dx.doi.org/10.5772/57066

could have been achieved by a moderate increase in the injection pressure at these stages. Therefore, the overall injectivity can be improved while sustaining the sequestration security, if the injection rate can be adjusted with respect to time such that the injection pressure levels off as it approaches the fracture pressure and is maintained at that level during the later injection stage. Such a scenario is identified as the constant pressure injection (CPI) since the injection pressure is more or less maintained at a constant level. The concept of CPI fits perfectly into the category of the development of a "smart" injection well for SAGCS.

5.1. Method for designing constant pressure injection (CPI)

The optimization problem setup for CPI is rather straightforward. Before the optimization, a threshold pressure (the pressure limit chosen based on the formation's fracture pressure and other engineering concerns and regulations) is chosen as the optimization constraint. Since it is assumed that the injection rate is the only quantity to be adjusted for CPI, it becomes the design variable. The optimization is then carried out to minimize the fitness function defined by equation (9).

$$\text{fitness function} = \text{modified injectivity} = \frac{\left| p_{\text{threshold}} - p_{injection}(Q_{CO2}) \right|}{Q_{CO2}} \tag{11}$$

When the fitness function in equation (9) approaches zero, CPI operation is obtained and the corresponding injection scenario can then be determined. The optimization design of CPI operation is carried out using GA-TOUGH2. The optimization is essentially a solution-searching problem utilizing the GA optimization technique.

Unlike the optimization of the WAG operation, a new challenge emerges, namely how to describe the CO_2 injection rate as a time-dependent continuous function with limited discrete data. The concept of Bézier curve is introduced to address this problem. A Bézier curve is a parametric curve frequently used in computer graphics and related fields [15],[16]. It is defined by a set of control points, and uses them as coefficients of a certain polynomial to describe continuous curves. The control points of a Bézier curve can be denoted as P_0 through P_n, with (n-1) being the order of the Bézier curve. The order determines the complexity of the Bézier curve. A Bézier curve provides a simple means of creating arbitrary complex curves. A generalized mathematical expression of an n^{th} order Bézier curve is given as:

$$B(t) = \sum_{i=0}^{n} \binom{n}{i} (1-t)^{n-i} t^i P_i \tag{12}$$

where (n,i) is the binomial coefficient, P_i is the i^{th} control point defined prior to the curve's generation, and t is a variable defined on [0, 1]. Defining four control points as P_1, P_2, P_3, and P_4, an example of a cubic Bézier curve is shown in Figure 26.

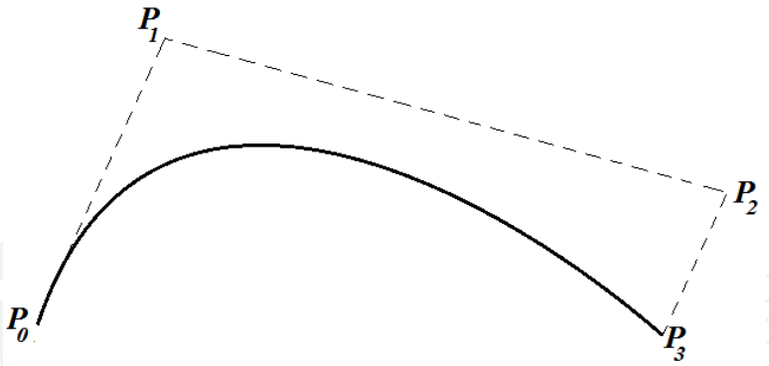

Figure 26. Graph of a cubic (3rd order) Bézier curve

In our work, each CO_2 injection scenario is described by a cubic Bezier curve. The CO_2 injection is a time dependent function of mass flow rate. Discretization of the injection with respect to time is needed to make the problem tractable for numerical simulation. With the discretization, CO_2 injection can be represented by step-functions for each time interval, and ultimately approximates the smooth injection as the time interval becomes small enough. The injection rate for each discrete time step is described at the midpoint of the interval, known as the sample point. Coordinates of other control points are arbitrarily generated for each GA individual. Any arbitrary CO_2 injection scenario can be generated by letting the parameter t increase from 0 to 1.

The design of CPI operation employs the identical hypothetical generic saline formation modeled for the optimization of WAG injection with a horizontal injector, as shown previously in Figure 20. All hydrogeological properties and numerical parameters remain unchanged. A threshold pressure of 180 bar is set for the maximum allowable injection pressure, with the assumption of a 50% increase from the initial pressure (120 bar). As mentioned earlier, the choice of threshold pressure is based on considerations of various aspects, such as the fracture pressure, injection regulation, safety factor, and risk analysis. The injection rate is allowed to vary between 0 kg/s and 150 kg/s, and the injection lasts for five years. The injection pressure response and the corresponding time-dependent injection rate of the optimized CPI operation are given in Figure 27. Two CGI cases, one with high injection rate (44 kg/s) and one with low rate (24 kg/s), are also included in these figures for comparison.

Several conclusions can be drawn by carefully examining the results of Figure 27. First, the injection pressure (green curve in Figure 27) is well behaved under the constraint of the threshold pressure. It increases rapidly at the early stage of the injection (on the order of days), and levels off as it approaches 180 bar. This is exactly the desired behavior of injection pressure response. Starting from 28 kg/s, the injection rate keeps increasing with the stabilized injection pressure. This means that the well injectivity gradually improves as CO_2 injection continues. Improved injectivity indicates more injected CO_2 after five years of operation. A direct indicator of the success of the designed CPI operation is the five-year average injection rate of 38 kg/s (compared to 34 kg/s for CGI operation). Second, both CGI operations first give an increase and then a decrease in injection pressure response, validating our previous conclu-

http://dx.doi.org/10.5772/57066

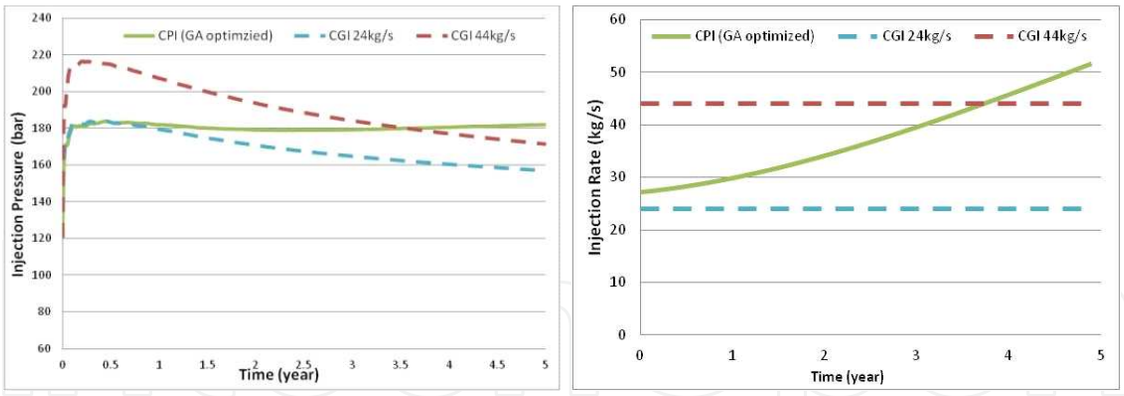

Figure 27. Injection pressure and injection rate of the optimized CPI operation, and its comparison with low-rate CGI and high-rate CGI

sion. Similar behavior of loss in injectivity has also been suggested by Burton et al. [17]. It can be seen that the injection pressure reaches about 220 bar with the high-rate CGI operation (44 kg/s), which is a 40 bar overshoot above the threshold pressure. Additionally, such pressure overshoot lasts for over 3.5 years before the injection pressure falls below 180 bar. Such large and prolonged pressure overshoot poses a significant risk to the formation's integrity. On the other hand, it is also seen that the injection pressure response with the low-rate CGI operation (24 kg/s) falls far below the threshold pressure after it peaks at the early stage. Although the integrity of the formation is not threatened, the injectivity has been severely compromised under such a low injection rate. Thus, only the CPI operation gives the optimal injection pressure management, which realizes the best injectivity while ensuring the injection safety by keeping the pressure always below the fracture pressure of the formation. Again, GA-TOUGH2 has successfully designed the CPI operation for a given pressure constraint.

6. Performance optimization of a multi-well system

It is likely that only a system of multiple injection wells would deliver enough injectivity for industrial level SAGCS. In the presence of multiple wells, the low compressibility of brine can potentially result in strong interference in the pressure generated by each well. This then brings up the question of how much the pressure interference is generated in a multi-well injection system, and how the injection wells should be placed to minimize interference. Two types of interference have been identified in a multi-well injection system, namely the CO_2 front interference and the pressure front interference, as described by Eccles et al. [18]. Neglecting complex in situ interactions such as phase shifting and mineralization, the interface between injection wells can be roughly estimated by superposition of the quantities from each single-well injection. If the aquifer is assumed to be relatively isotropic in its hydrogeological properties, Darvish et al. have shown that placing the wells on corners of regular polygons is preferred for uniform interference among wells [19]. Following such angular distribution of injection wells, the distance between the wells becomes the design variable for optimization. A four-well injection system is first considered to investigate the interference of plume

migration and pressure disturbance between the wells. Afterwards, a two-well injection system is considered to study the relationship between well spacing and injectivity.

6.1. Four-well injection system

A hypothetical saline aquifer with dimensions of 4000 m × 4000 m × 70 m is modeled for this study. Generic hydrogeological properties and reservoir conditions similar to those used in the WAG operation study are assigned. The computational mesh is refined near the injection wells for accurate capture of the interference. Four cases with different inter-well distance are considered, in which injection wells are 600 m, 800 m, 1200 m, and 1600 m diagonally apart. The computational domains for the four cases are shown in Figure 28.

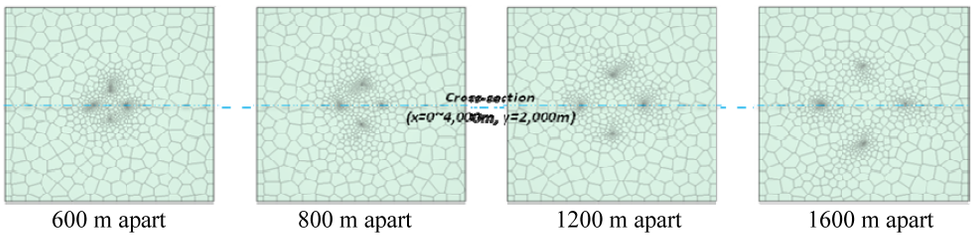

Figure 28. Computational domain of four-well injection systems with various inter-well distances

CO_2 is injected at a constant rate of 5 kg/s in each well. Mean injection pressure and gas saturation underneath the caprock after five years of injection are examined along the cross section indicated in Figure 29. The pressure response and CO_2 saturation curves are shown and compared in Figure 29 and Figure 30 respectively.

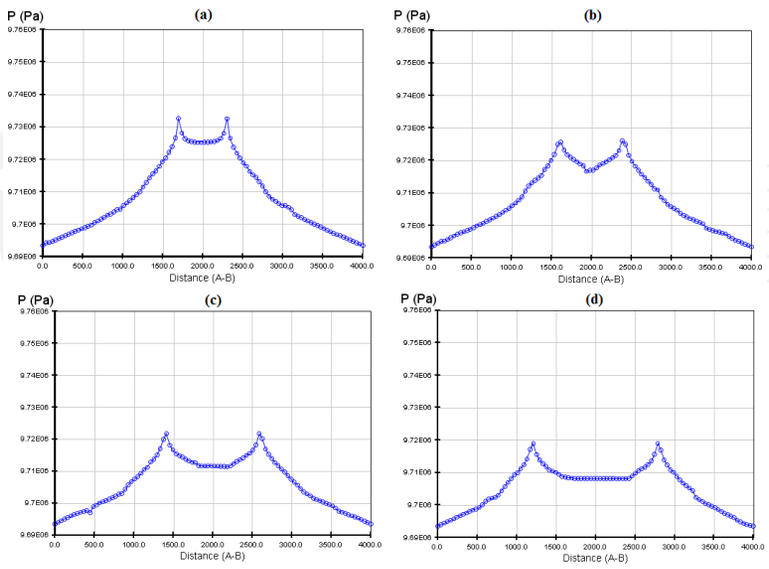

Figure 29. Pressure profile at the cross-section: wells (a) 600 m apart, (b) 800 m apart, (c) 1200 m apart, and (d) 1600 m apart

http://dx.doi.org/10.5772/57066

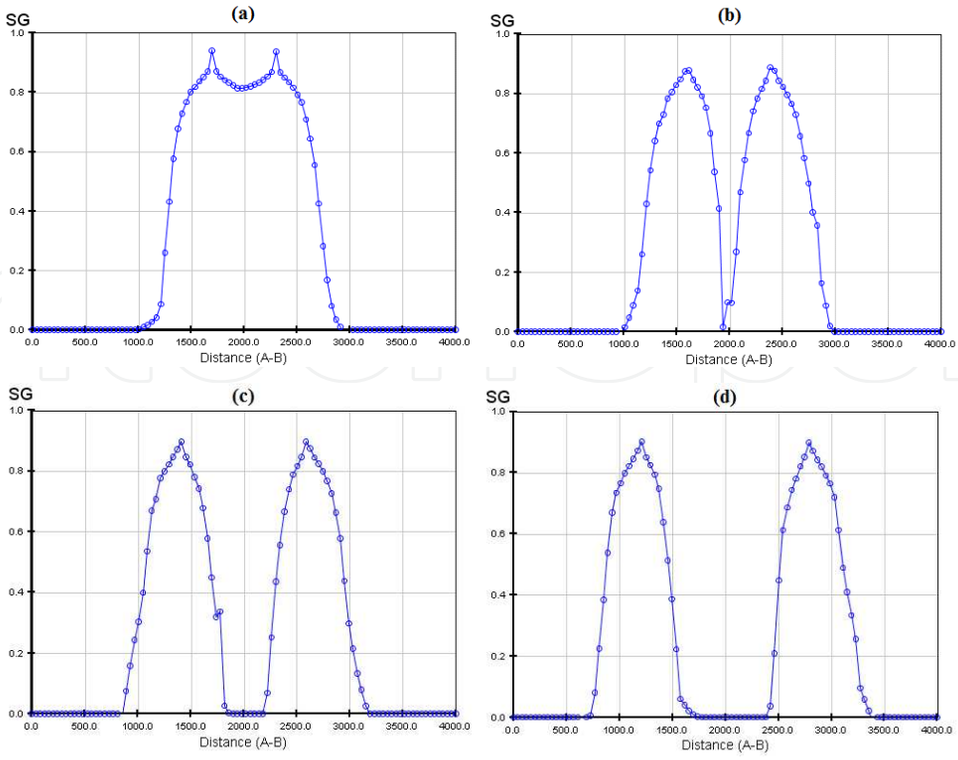

Figure 30. Gas saturation underneath the caprock at the cross-section: wells (a) 600 m apart, (b) 800 m apart, (c) 1200 m apart, and (d) 1600 m apart

The following conclusions can be reached based on the results shown in Figure 29 and Figure 30. First, well injectivity can be greatly improved by utilization of a multi-well injection system. The four-well system considered delivers CO_2 at total rate of 20 kg/s with no greater than 0.4% increase in reservoir pressure. This is orders of magnitude smaller than that of a single injection well for the same injection rate. This shows the technical benefit of utilizing a multi-well injection system for industrial level SAGCS. Second, well interference is prominent due to the presence of multiple injection wells. In Figure 29, the injection induced pressure elevation is 0.38% of the reservoir mean pressure for the case of 600-m inter-well spacing, while it drops to only 0.26% for the case of 1600-m inter-well spacing. That is to say, pressure interface is about 32% stronger when injection wells are 600 m apart compared to when they are 1600 m apart. The interference of the CO_2 plume is also seen in Figure 30. Third, comparison of Figure 29 and Figure 30 shows that the pressure interference is predominantly responsible for the compromised injectivity in a multi-well injection system. Plume interference can be easily avoided by moderately increasing the well spacing. For instance, plume interference is prominent for 600-m inter-well spacing, but almost disappears for 800-m inter-well spacing (as shown in Figure 30). On the other hand, the pressure interference remains persistent, which requires at least 1600-m inter-well spacing to become insignificant. However, large spacing between injection wells will result in greater land use. Therefore, optimal placement of wells is desirable to achieve an acceptable pressure and capacity interference as well as land use.

6.2. Two-well injection system

Because pressure interference is largely responsible for compromised injectivity of a multi-well injection system, in this section we examine the relationship between inter-well spacing and well injectivity. A half domain with dimensions 50000 m × 25000 m × 100 m is modeled. The computational domain is horizontally discretized by a uniform quadrilateral mesh with resolution of 200 m × 200 m and 500 m × 500 m. Two injection wells are assigned symmetrically at the center of the domain. The distance between these two injection wells is allowed to change freely and is considered as a design variable for the GA optimizer. Like the previous investigations of the four-well injection system, the injection operation is assumed to last for five years. Three cases with different injection rates and model parameters are considered, summarized in Table 10.

	Case #1	**Case #2**	**Case #3**
Single Well Injection Rate	2 kg/s	16 kg/s	16 kg/s
Hydrogeological Properties	Generic formation	Generic formation	Generalized Utsira formation
Mesh Resolution	200 m × 200 m	500 m × 500 m	500 m × 500 m

Table 10. Optimization cases for two-well injection system.

Denoting the injection pressure of the two-well injection system as $P_{two\text{-}well}$, and the injection pressure of the single-well injection system as $P_{single\text{-}well}$, the pressure difference ΔP between $P_{two\text{-}well}$ and $P_{single\text{-}well}$ is chosen as the fitness function. GA-TOUGH2 is employed to determine the minimal inter-well distance for a designated value of ΔP. For each case in Table 10, three optimization criteria are considered, namely ΔP being no greater than 0.1%, 0.5%, and 2% of $P_{single\text{-}well}$. The value of ΔP is examined and optimization is performed at the end of the five-year injection. In addition, well injectivity loss due to the pressure interference is also evaluated for the optimal well spacing given by GA-TOUGH2. Recalling the definition of well injectivity, equation (11), the injectivity loss of the two-well injection system can be evaluated as:

$$\begin{aligned}\text{injectivity loss} &= \text{injectivity}_{\text{two-well system}} - \text{injectivity}_{\text{single-well system}} \\ &= \left(\frac{Q_{CO2}}{P_{\text{two-well}} - P_{\text{reservior}}} - \frac{Q_{CO2}}{P_{\text{single-well}} - P_{\text{reservior}}} \right) \Bigg/ \frac{Q_{CO2}}{P_{\text{sin}\,glewell} - P_{reservior}} \\ &= \frac{P_{\text{two-well}} - P_{\text{single-well}}}{P_{\text{single-well}} - P_{\text{reservior}}}\end{aligned} \tag{13}$$

where Q_{CO2}, $P_{two\text{-}well}$, and $P_{single\text{-}well}$ are as defined earlier. The optimization results are summarized in Table 11.

Several conclusions can be reached after careful examination of the optimization results in Table 11. First, it should be noted that the total amount of injected CO_2 is doubled from the

http://dx.doi.org/10.5772/57066

	Case #1		Case #2		Case #3	
Optimization Criteria	Inter-well Distance	Injectivity Loss	Inter-well Distance	Injectivity Loss	Inter-well Distance	Injectivity Loss
$\Delta P < 0.1$ % *Psingle-well*	5.4 km	-2.84%	32 km	-0.94%	14 km	-2.53%
$\Delta P < 0.5$ % *Psingle-well*	1.8 km	-12.76%	19 km	-4.54%	below mesh resolution	
$\Delta P < 2$ % *Psingle-well*	below mesh resolution		6.5 km	-28.57%	below mesh resolution	

Table 11. Optimal inter-well spacing and injectivity tradeoff for three cases under three optimization criteria.

single-well injection case for all optimization cases due to the presence of the second injection well. Second, the results show that for Case #1, pressure interference can be substantially reduced for ($\Delta P < 0.1\%$ of $P_{single\text{-}well}$) by placing injection wells 5400 m apart, for ($\Delta P < 0.5$ % of $P_{single\ well}$) by placing injection wells 1800 m apart, and for ($\Delta P < 2$ % of $P_{single\ well}$) by placing injection wells less than 200 m apart. The relative ease of mitigating the pressure interface for Case #1 can be explained by its low injection rate of 2 kg/s per well. However, a low injection rate leads to low injection pressure, which in turn makes the injectivity more sensitive to the injection pressure. 2.84% and 12.76% injectivity losses are found for Case #2 and Case #1 respectively. Case #2 is similar to Case #1 except for the significantly increased injection rate of 16 kg/s per well. Accordingly, the inter-well distance increases to meet the optimization criteria. It is estimated that at least 32 km, 19 km, and 6500 m distance between the wells is needed to realize the three levels of avoidance in pressure interference respectively. An encouraging result is that the injectivity loss for Case #2 is significantly smaller than that for Case #1. Such reduction in injectivity loss also implies the dominant role of injection rate when evaluating the injectivity of a multi-well injection system. Therefore, simply increasing the injection rate can be a direct and effective means to mitigate the injectivity loss due to pressure interference. However, it is worth noting that even for the reasonable avoidance of pressure interference in Case #2, the wells need to be placed 6500 m apart, which is still a significant distance considering land use. The exacerbated injectivity loss of 28.57% may also pose concerns on injection well performance. In Case #3, the hydrogeological properties of the Utsira sandstone formation are assigned to the modeled domain to obtain some real-life sense of the performance of a multi-well injection system. Due to the improved reservoir conditions, i.e., higher porosity and permeability, the inter-well distance to achieve the significant avoidance of pressure interference decreases greatly from 32 km in Case #2 to 14 km in Case #3. Moreover, the required inter-well distances even fall under the mesh resolution, i.e., less than 500 m, for the other less rigorous criteria in pressure interference. This suggests the great potential of implementing a multi-well injection system for the SAGCS of the Utsira formation without concern over large pressure interference. These results also show the promise of implementing a multi-well injection system for other large-scale saline formations.

7. Concluding remarks

In this chapter, the development of genetic-algorithm based optimizations has been described, integrated into the DOE multiphase flow and heat transfer numerical simulation code TOUGH2. The new code has been designated GA-TOUGH2. GA-TOUGH2 has the ability to determine optimal reservoir engineering techniques for improved CO_2 storage efficiency in saline aquifer carbon sequestration. Using GA-TOUGH2, the feasibility and technical benefits of adopting water-alternating-gas (WAG) injection technique has been investigated for SAGCS. In addition, problems such as optimal injection pressure management in SAGCS and injection well placement in a multi-well injection system have been investigated for the purpose of achieving higher storage efficiency and safer sequestration. Encouraging results have been obtained from all these optimization studies. Validated GA-TOUGH2 thus offers an innovative platform which holds great promise in studying a host of optimization/design problems for geological carbon sequestration.

As recommendations for the future work, more complex optimization studies could be performed to address a broader set of optimization problems, such as non-uniform WAG injection and maximization of capillary trapping. Some analytical solutions could be derived for more fundamental understanding of the WAG injection. Multi-objective GA optimization should also be introduced to obtained a higher level of optimization capability with consideration of multiple fitness functions. Additional real-life SAGCS projects such as the ADM project and FutureGen 2.0 should be continually studied over the years as more detailed field data become available. Optimization studies for these large-scale SAGCS projects should be performed for greater storage efficiency and reduced plume migration. GA-TOUGH2 should also be considered for the study of other aspects of GCS, such as enhanced oil or gas recovery in combination with carbon sequestration.

Acknowledgements

Financial support for this work was provided by the Consortium for Clean Coal Utilization (CCCU) at Washington University in St. Louis, MO, USA.

Author details

Ramesh K. Agarwal and Zheming Zhang

Department of Mechanical Engineering and Materials Science, Washington University in St. Louis, St. Louis, USA

References

[1] Pruess K. TOUGH2: A General Numerical Simulator for Multiphase Fluid and Heat Flow, Lawrence Berkeley Laboratory Report LBL-29400, California: Berkeley; 1999.

[2] Pruess K., Oldenburg C., and Moridis G. TOUGH2 User's Guide, Version 2.0 (revised), Lawrence Berkeley Laboratory Report LBL-43134, California: Berkeley; 2011.

[3] Genetic algorithm, Wikipedia website, http://en.wikipedia.org/wiki/Genetic_algorithm (accessed 24 May 2013).

[4] Goldberg D.E. Genetic Algorithms in Search, Optimization & Machine Learning. Addison-Wesley; 1989.

[5] Zhang Z. and Agarwal R. Numerical Simulation and Optimization of CO_2 Sequestration in Saline Aquifers. Computers & Fluids 2012; 16 (4) 891-899.

[6] Zhang Z. Numerical Simulation and Optimization of CO_2 Sequestration in Saline Aquifers. Ph.D dissertation. Washington University in St. Louis, USA; 2013.

[7] Tchelepi H., Durlofsky L., and Aziz K. A Numerical Simulation Framework for the Design, Management and Optimization of CO_2 Sequestration in Subsurface Formations. Global Climate and Energy Project (GCEP) Report, Stanford, 2009.

[8] Orr L. Carbon Capture and Sequestration: Where do We Stand? Presentation at NAE/AAES Convocation, Washington DC, 19 April, 2010.

[9] Bryant S.L., Lakshminarasimhan S., and Pope G.A. Buoyancy-dominated Multi-Phase Flow and Its Effect on Geological Sequestration of CO_2. Society of Petroleum Engineers Journal 2008; 447-454.

[10] Leonenko Y. and Keith D.W. Reservoir Engineering to Accelerate the Dissolution of CO_2 Stored in Aquifers. Environmental Science & Technology 2008; 42 2742-2747.

[11] Jikich S.A., Sams W.N., Bromhal G., Pope G., Gupta N., and Smith D.H. Carbon Dioxide Injectivity in Brine Reservoirs Using Horizontal Wells. In: 2nd Annual Conference on Carbon Sequestration, May 2003, Pittsburgh, PA, USA.

[12] Hassanzadeh H., Pooladi-Darvish M., and Keith D.W. Accelerating CO_2 Dissolution in Saline Aquifers for Geological Storage - Mechanistic and Sensitivity Studies. Energy and Fuels 2009; 23 3328-3336.

[13] Nasir F.M. and Chong Y.Y. The Effect of Different Carbon Dioxide Injection Modes on Oil Recovery. International Journal of Engineering & Technology 2009; 9 66-72.

[14] Audigane P., Gaus I., Czernichowski-Lauriol I., Pruess K., and Xu T., Two-Dimensional Reactive Transport Modeling of CO_2 Injection in a Saline Aquifer at the Sleipner Site. American Journal of Science 2007; 307 974-1008.

[15] Farin G. Curves and Surfaces for Computer-Aided Geometric Design, Fourth Edition. Academic Press, Waltham; 1996.

[16] Bézier curve, Wikipedia website, http://en.wikipedia.org/wiki/B%C3%A9zier_curve (accessed 24 May 2013).

[17] Burton M., Kumar N., and Bryant S.L. CO_2 Injectivity into Brine Aquifers: Why Relative Permeability Matters as Much as Absolute Permeability. Energy Procedia 2009; 1 (1) 3091-3098.

[18] Eccles J., Chandel M., and Pratson L. Large Scale Carbon Storage Deployment: Effects of Well Spacing on Geosequestration Site Costs and Capacity Estimates. In: 10th Annual Conference on Carbon Capture & Sequestration, May 2011,Pittsburgh, PA, USA.

[19] Pooladi-Darvish M., Moghdam S., and Xu D. Multiwell Injectivity for Storage of CO_2 in Aquifers. Energy Procedia 2011; 4 4252-4259.